REFERENCES

D. Heidrich, W. Kliesch, and W. Quapp, 'Properties of Chemically Interesting Potential Energy Surfaces', Springer-Verlag, Berlin, 1991; D. Heidrich (ed.), 'The Reaction Path in Chemistry: Current Approaches and Perspectives', Kluwer, Dordrecht, 1995.
M. L. McKee and M. Page, *Rev. Comput. Chem.*, 1993, **4**, 35–65.
H. B. Schlegel, in 'Modern Electronic Structure Theory', ed. D. R. Yarkony, World Scientific Publishing, 1995, pp. 459–500.
M. A. Collins, *Adv. Chem. Phys.*, 1996, **93**, 389–453.
J. Pancir, *Coll. Czech. Chem. Commun.*, 1975, **40**, 1112–1118; M. V. Basilevsky and A. G. Shamov, *Chem. Phys.*, 1981, **60**, 347–358; D. K. Hoffman, R. S. Nord, and K. Ruedenberg, *Theor. Chim. Acta*, 1986, **69**, 265–279.
K. Fukui, *Acc. Chem. Res.*, 1981, **14**, 363–368.
W. Quapp and D. Heidrich, *Theor. Chim. Acta*, 1984, **66**, 245–260.
J. J. P. Stewart, L. P. Davis, and L. W. Burggraf, *J. Comput. Chem.*, 1987, **8**, 1117–1123; S. A. Maluendes and M. J. Dupuis, *J. Chem. Phys.*, 1990, **93**, 5902–5911; M. S. Gordon, G. Chaban, and T. Taketsugu, *J. Phys. Chem.*, 1996, **100**, 11512–11525.
K. Bolton, W. L. Hase, and G. H. Peslherbe, in 'Modern Methods in Multidimensional Dynamics Computations in Chemistry', ed. D. L. Thompson, World Scientific Publishing, 1998.
W. H. Press, B. P. Flannery, S. A. Teukolsky, and W. T. Vetterling, 'Numerical Recipes', Cambridge University Press, 1989.
C. W. Gear, 'Numerical Initial Value Problems in Ordinary Differential Equations', Prentice-Hall, 1971.
K. Ishida, K. Morokuma, and A. Komornicki, *J. Chem. Phys.*, 1977, **66**, 2153–2156; M. W. Schmidt, M. S. Gordon, and M. Dupuis, *J. Am. Chem. Soc.*, 1985, **107**, 2585–2589.
K. Müller and L. D. Brown, *Theor. Chim. Acta*, 1979, **53**, 75–93.
(a) M. Page and J. W. McIver, Jr., *J. Chem. Phys.*, 1988, **88**, 922–935; (b) M. Page, C. Doubleday, and J. W. McIver, Jr., *J. Chem. Phys.*, 1990, **93**, 5634–5642; (c) J. Q.-Sun and K. Ruedenberg, *J. Chem. Phys.*, 1993, **99**, 5269–5275.
C. Gonzalez and H. B. Schlegel, *J. Chem. Phys.*, 1989, **90**, 2154–2161; *J. Phys. Chem.*, 1990, **94**, 5523–5527.
K. K. Baldridge, M. S. Gordon, R. Steckler, and D. G. Truhlar, *J. Phys. Chem.*, 1989, **93**, 5107–5119; V. S. Melissas, D. G. Truhlar, and B. C. Garrett, *J. Chem. Phys.*, 1992, **96**, 5758–5772.
C. Gonzalez and H. B. Schlegel, *J. Chem. Phys.*, 1991, **95**, 5853–5860.
P. G. Jasien and R. Shepard, *Int. J. Quantum Chem., Quantum Chem. Symp.*, 1988, **22**, 183–198.
R. Elber and M. Karplus, *Chem. Phys. Lett.*, 1987, **139**, 375–380.
L. L. Sacho and M. I. Bán, *Theor. Chim. Acta*, 1992, **83**, 433–440.
P. Ayala and H. B. Schlegel, *J. Chem. Phys.*, 1997, **107**, 375–384.
E. B. Wilson, J. C. Decius, and P. C. Cross, 'Molecular Vibrations', McGraw-Hill, New York, 1955.
A. G. Basoul and H. B. Schlegel, *J. Chem. Phys.*, 1997, **107**, 9413–9417.
P. Valtazanos and K. Ruedenberg, *Theor. Chim. Acta*, 1986, **69**, 281–307.
J. Baker and P. M. W. Gill, *J. Comput. Chem.*, 1988, **9**, 465–475.
P. Jørgensen, H. J. Jensen, and T. Helgaker, *Theor. Chim. Acta*, 1988, **73**, 55–65.
H. B. Schlegel, *Theor. Chim. Acta*, 1992, **83**, 15–20.
J. Q.-Sun and K. Ruedenberg, *J. Chem. Phys.*, 1993, **98**, 9707–9714.
K. Bondensgard and F. Jensen, *J. Chem. Phys.*, 1996, **104**, 8025–8031.

Reaction Path Hamiltonian

See ***Reaction Path Following***.

Reaction Path Hamiltonian and its Use for Investigating Reaction Mechanisms

Elfi Kraka

Göteborg University, Sweden

Abbreviations

LAM = large amplitude motion; RP = reaction path; RPH = reaction path Hamiltonian; RSH = reaction surface Hamiltonian; SAM = small amplitude motion; SRP = specific reaction parameter; SRPH = solution reaction path Hamiltonian.

1 INTRODUCTION

Key issues in chemistry are the description and understanding of mechanism and dynamics of chemical reactions. In principle, this understanding can be obtained by designing and carrying out suitable experiments. However, in practice it is rather difficult to get a detailed mechanistic and dynamic description of even the simplest chemical reactions. This has to do with the fact that apart from reactants, products, and possible stable intermediates, all other molecular forms encountered during a reaction have such a short lifetime that standard experimental means are not sufficient to detect and describe them. Progress in modern laser spectroscopy seems to provide an access to transient species with lifetimes in the pico- to femtosecond region;[1] however, much more development in this research area is needed to make this approach a standard experimental method for describing reaction mechanism and reaction dynamics in detail.

Today, computational investigations utilizing state-of-the art methods of quantum chemistry, in particular *ab initio* methods, provide the major source of knowledge on reaction mechanism and reaction dynamics. For this purpose, the interactions between the atomic and/or molecular species involved in a reaction are calculated and analyzed with the help of *ab initio* methods.

1.1 The Potential Energy Surface

Atomic or molecular interactions are investigated on the basis of the *Born–Oppenheimer approximation*, which separates electronic and nuclear motions and is the starting point for getting an electronic wave function and an electronic interaction energy for a clamped nuclei situation. For every possible configuration of the nuclei of a molecule, a potential energy can be determined with the help of electronic structure calculations (*ab initio*, semiempirical). The function that describes how the potential energy V changes as the nuclei move relative to one another defines the *potential energy hypersurface* (PES), which is the many-dimensional generalization of the well known diatomic potential energy curve. Hence, a direct consequence of the Born–Oppenheimer approximation is the concept of PES,[2,3] which is used to describe changes in the potential energy of a reaction complex during the course of a chemical reaction.

Knowledge about the PES of a given reaction system is essential for investigating reaction mechanism and reaction dynamics and, thus the PES plays a central role in our understanding of chemical reactivity.[2] The PES function $V(\boldsymbol{R})$ for a reaction complex composed of K atoms depends on $(3K - L)$ internuclear coordinates $\boldsymbol{R} = (R_1, R_2, \ldots, R_{3K-L})$ where L is the number of overall translations and external rotations of the reaction complex ($L = 6$ for a nonlinear, $L = 5$ for a linear reaction complex), which are of no relevance for the description of the electronic interactions between the reaction partners. Calculation and characterization of the multi-dimensional function $V(\boldsymbol{R})$ presents one of the major challenges in modern quantum chemistry. Despite the rapid progress in *ab initio* methodology and computer techniques since the mid-1970s, there remain major obstacles when determining $V(\boldsymbol{R})$: (1) The calculation of $V(\boldsymbol{R})$ to chemical accuracy, i.e., better than 1 kcal mol^{-1}, remains an elusive goal for any save the simplest reaction systems. (2) A general procedure for obtaining accurate, analytic representations of $V(\boldsymbol{R})$ has not yet been developed, and (3) the complex, multi-dimensional function $V(\boldsymbol{R})$ is not in a form that can readily be analyzed and used to extract simple, useful, yet theoretically sound, chemical concepts.

1.2 The Mountaineer's Terminology for PES Descriptions

From daily life, we are familiar with gravitational potential energy experienced when climbing up a mountain path to cross a mountain region with high peaks. Such a path always follows a mountain valley up to a pass between two peaks and, then, descends through a second valley on the other side of the mountain region. The mountaineer's terminology and his experience with gravitational potential energy is used when describing a multi-dimensional PES. Accordingly, one speaks of energy wells (minima), energy peaks or hilltops (maxima), energy valleys, energy passes (saddlepoints), etc., when explaining the features of a PES.

The chemically relevant parts of the PES are minima, valleys, and a *saddlepoint* between two valleys. The location of the energy minima in $(3K - L)$-dimensional space determines geometries and energies of reactants and products. The curvature in the various directions of space at a minimum, i.e., the steepness of the walls of an energy well, is related to the vibrational properties of a molecule, such as the harmonic force constants and the corresponding vibrational frequencies. Two energy minima on different sides of an energy saddlepoint are connected by two valley paths that start at the reactant or product minimum and end at the saddlepoint. Together the valley paths form a contiguous path from reactants to products on the PES, which is called the reaction path (RP).

The saddlepoint has the property of being an energy maximum in the path direction, but a minimum in all other directions perpendicular to the RP. The chemical significance of the saddlepoint is that it is the location of the transition state (TS) of the reaction leading from reactants to products. The energy of the TS determines the barrier height and thus whether a reaction takes place (low barrier) or not (high barrier). Molecular trajectories that cross the saddlepoint region from the reactant to the product minimum side are unlikely to return to the reactant side. Hence, the saddlepoint is a dynamic bottleneck, which will particularly be true if the barrier is high and reaction probability and reaction rate are low.

1.3 The Dimensionality Dilemma of PES Studies

It has been estimated that for the description of the PES of a reaction system with K atoms about 10 points are required for each coordinate to characterize PES properties in the direction of this coordinate and therefore about 10^{3K-L} *ab initio* calculations are needed for a reasonable PES description.[4] In the case of a three-atom system ($K = 3, L = 6$) this would mean 10^3 calculations; $K = 6$ and $L = 6$ requires 10^{12} *ab initio* calculations. Even with modern computer technology this is not feasible and, therefore, it is an elusive goal to determine the PES function $V(\boldsymbol{R})$ for larger reaction systems.

Out of this dimensionality dilemma, a strategy for systematically simplifying the problem of determining the complete PES of a reaction system has been developed: (1) Determination of the PES is constrained to that part which is energetically relevant for the reaction in question. In particular, one concentrates on the RP (and the associated reaction valleys), that connects reactants, TS, and products (static reduction). (2) The dynamic investigation is restricted to the translational mode along the RP and just those large amplitude modes (LAM) that strongly couple to the translational mode (dynamic reduction).

The first idea emerged when it became obvious that chemical reactions are local phenomena, i.e., only a limited number of atoms is involved in the actual reaction. For example, just two or three atoms participate in most cases of bond breaking or forming processes while the rest of the molecule is only slightly influenced. Accordingly, chemists usually describe a reaction in terms of a local coordinate such as a bond distance or an approach parameter. This leads to one-dimensional simplifications of the PES that give the energy change for a specific reaction process in terms of the particular local coordinate associated with the reaction (Figure 1).

Although representations such as that of Figure 1 can be found in all chemical textbooks and are the basis for a qualitative or semiquantitative analysis of chemical reaction mechanism, they contain two serious simplifications: (a) For most reactions of a polyatomic reaction complex, the RP cannot be described using a single coordinate. The RP is curved in the $(3K - L)$-dimensional configuration space and to describe the curvature correctly one needs nearly all the coordinates, where of course some coordinates may be more

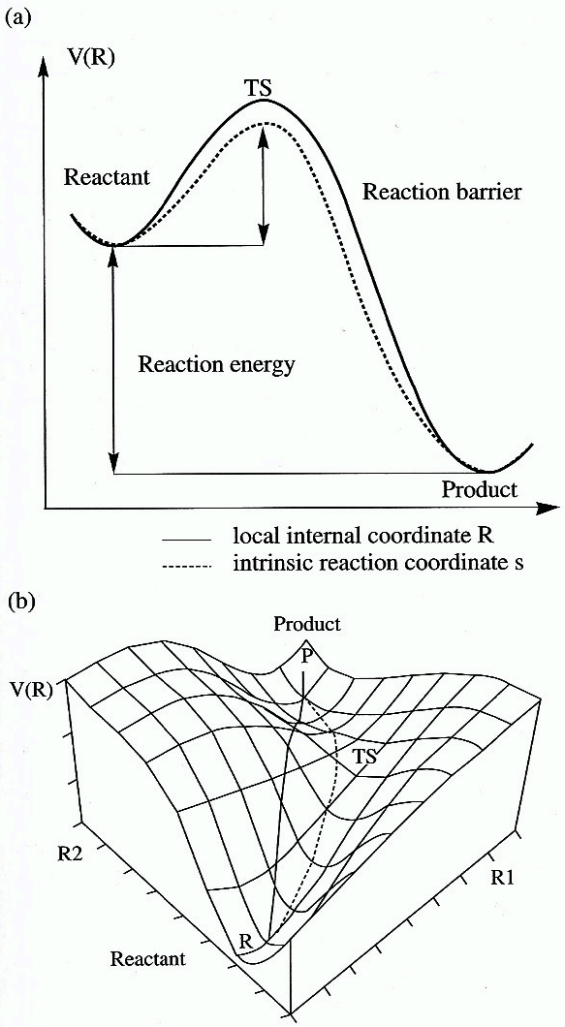

Figure 1 (a) Energy profile of a standard chemical reaction involving reactant, transition state (TS), and product given as a function of a local internal coordinate R (solid line) and the correct (intrinsic) reaction coordinate s (dashed line). (b) Perspective drawing of the corresponding PES. Reproduced with permission from H. B. Schlegel, *Adv. Chem. Phys.*, **27**, 249–286. Copyright (1987) John Wiley & Sons

important than others in the description. (b) Given a set of $(3K - L)$ internal or Cartesian coordinates, only the location of the stationary points can uniquely be determined on the PES while the RP connecting the stationary points depends on the coordinates chosen, i.e., its unique definition requires special coordinates leading to an intrinsic *reaction coordinate* (IRC) as indicated in Figure 1.[5] If the RP is described by the correct IRC, one will often find an energetically lower TS than that obtained for a RP calculated with a local internal coordinate R (Figure 1).

Points (a) and (b) are responsible for the fact that most mechanistic work based on quantum chemical calculations concentrates on reactants, TS, and products rather than calculating the whole RP. As mentioned above, reactants, TS, and products occupy minima and (first-order) saddlepoints on the PES, which have the property of being independent of the coordinates (e.g., Cartesian or internal) chosen for the description of the reaction complex. Reliable calculations of the properties of reactants, TS, and products lead to a determination of reaction barrier and reaction energy, reveal typical geometry changes during the reaction, and provide a first insight into the electronic structure of the reaction complex. Hence, localization and investigation of the stationary points of the PES along a RP is a reasonable starting point for the description and understanding of reaction mechanism.

1.4 Methods for Investigating the PES

A hierarchy of approximate methods for describing the PES region, which is relevant for a given reaction, has been developed to compromise between the dimensionality problem of a complete PES investigation and the need for reliable mechanistic and dynamic insight into a chemical reaction.

Investigation of the Stationary Points along the RP: The energetics, geometrical changes, and changes of other properties taking place during a chemical reaction are determined by analyzing the corresponding properties of the *stationary points*. Qualitative insight into the reaction dynamics is possible. Computational costs are feasible for relatively large reaction systems even when using rather expensive *ab initio* methods of high accuracy and reliability. However, a prerequisite for this and any of the following approximations is that the location of the TS (saddlepoint) is correctly determined.

Investigation of the total RP by using appropriate coordinates: The RP is explored by proceeding on it in a stepwise manner using appropriate mathematical techniques and an appropriate mass-weighted coordinate system. Simplified, but useful, descriptions of the reaction dynamics become possible. Depending on the number of points calculated along the RP and the *ab initio* method used, computational costs are still tolerable.

Investigation of the reaction valley in the harmonic approximation: At each path point, the orthogonal directions to the RP are described by a quadratic (harmonic) approximation of the potential $V(\boldsymbol{R})$, which implies the calculation of the second derivatives of $V(\boldsymbol{R})$ with regard to the internal coordinates. A coupling of translational and vibrational motions of the reaction complex can be described, which is the basis for a more quantitative investigation of reaction mechanism and reaction dynamics.[4] Calculations can be done for most of the reaction systems considered by approach (2). Of course, a routine, inexpensive calculation of the matrix of second derivatives of $V(\boldsymbol{R})$ is desirable.

Investigation of the reaction valley by considering anharmonic corrections:[6] To calculate the correct shape of the reaction valley in directions orthogonal to the RP, third and fourth derivatives of $V(\boldsymbol{R})$ with regard to the internal coordinates $\boldsymbol{R}$ have to be calculated, which leads to a drastic increase of computational cost and limits this approach to relatively small reaction complexes.

Investigation of reaction surfaces and reaction hypersurfaces:[7,8] If the translational motion of the reaction complex couples with other LAMs of the complex, the RP can be sharply curved in the regions with strong coupling. The actual trajectory of the reaction complex deviates far from the RP and a correct dynamic description can only be achieved if the reaction valley is extended to a minimum energy reaction surface or hypersurface, which embeds all LAMs. Calculations needed to describe the reaction (hyper) surface can become rather expensive and, therefore, this approach is limited to

small reaction systems and low-dimensional reaction surfaces. *Investigation of larger regions or the complete PES*: This can be done by calculating extended point grids and fitting them to an analytical function that represents $V(\boldsymbol{R})$. Because of the large computational cost typical of this approach, it has been done for a limited number of rather small reaction systems comprising not much more than three or four heavy atoms.[2,9]

Investigations along the line of (3), (4), or (5) can be carried out with the *reaction path Hamiltonian* (RPH) of Miller, Handy, and Adams[4] or one of its extensions[6–8] since the RPH provides a basis for useful mechanistic and dynamic investigations of chemical reactions. The majority of these investigations is constrained to chemical reactions taking place in the gas phase, although extensions of the RPH concept to the solution phase have also been suggested and applied.[10] In the following, the methodology of the RPH approach is described.

2 METHODOLOGY

To apply the RPH one has to carry out the following calculations:

(1) Localization of the stationary points, i.e., minima and first order saddlepoint, on that part of the PES which is associated with the chemical reaction to be investigated.
(2) Following the RP stepwise from one stationary point to the next and calculating various properties of the reaction complex at the points along the path investigated.
(3) Calculation of the elements of the RPH, in particular couplings between vibrational modes (mode–mode couplings or Coriolis couplings) and couplings between the translational mode along the RP and vibrational modes (mode–reaction path couplings or curvature couplings).[4]
(4) Analysis of the information collected along the RP to get a description of the reaction mechanism.

Steps (1)–(4) constitute the first part of an investigation using the RPH, which is followed by further calculations needed to describe the dynamics of the reaction:

(5) Solution of the coupled equations of motion for the nuclear degrees of freedom of the reaction complex.
(6) Calculation of the rate constant by statistical averaging and summing-up of the probabilities of detailed state-to-state processes.

Steps (5) and (6) are discussed in ***Rates of Chemical Reactions; Transition State Theory;*** and ***Unimolecular Reaction Dynamics***. Here, the focus will be on the first four steps of the procedure outlined above.

2.1 Quantum Chemical Methods Used in Connection with the RPH

The basic requirement for a quantum chemical method to be used in connection with the RPH is that all points along the RP are consistently described. Accordingly, one might assume that high accuracy *ab initio* methods alone will lead to reliable results in connection with the RPH. Because of computational limitations, early work with the RPH was done with rather simple methods such as *Hartree–Fock* (HF) theory in connection with minimal or split valence basis sets. Reconsidering these investigations in the light of more elaborate investigations with correlation-corrected *ab initio* methods and larger basis sets, it is astonishing that many mechanistic and dynamic features of the reactions considered are correctly described at a low accuracy level. Hence, for many reactions a qualitative insight is gained by using methods such as HF/STO-3G, HF/3-21G or HF/6-31G(d,p).

More recent investigations with the RPH employ standard correlation-corrected methods such as Møller–Plesset (MP) *perturbation theory* (see ***Møller–Plesset Perturbation Theory***) at second or fourth order (MP2, MP4) or coupled cluster (CC) methods (see ***Coupled-cluster Theory***) in connection with DZP or TZP basis sets. The repertoire of methods has recently been extended by applying density functional theory (DFT) (see ***Density Functional Theory (DFT), Hartree–Fock (HF), and the Self-consistent Field***) and some convincing results have been published (see Section 3).

Because of cost considerations, researchers have tried to combine low level calculations that are used to follow the RP with high level calculations applied just to the stationary points along the RP. Truhlar and co-workers have worked out appropriate correction functions that adjust the potential, frequencies, moments of inertia, etc. obtained with a low level method to the high level results obtained at the stationary points (and some other points). These dual level descriptions have been found to improve the accuracy of reaction rate calculations.[11]

There is also work with the RPH based on semiempirical methods.[12] However, semiempirical methods are parametrized for equilibrium geometries and, accordingly, do not necessarily represent all parts of a reaction valley in a consistent way. Because of this, Truhlar and co-workers have proposed modifications of known semiempirical methods so that all their adjustable parameters are varied to reproduce experimental or *ab initio* data for specific reactions.[12] Since most of the semiempirical methods presently in use are based on the NDDO approach, the term specific reaction parameter NDDO model (NDDO–SRP) has been coined.[12] The SRP parametrization changes the NDDO model from being qualitatively incorrect to semiquantitatively accurate and, accordingly, provides a much cheaper basis to apply the RPH.

Both the dual-level descriptions and the NDDO–SRP approach have to be applied with care since they can lead to discontinuities and spurious minima in the PES function. Also, there are cases for which the reparametrization of a NDDO method is too difficult to provide more than just a qualitative insight into the reaction dynamics.[13] Clearly, dual-level description and NDDO–SRP methods are only of limited value for a detailed investigation of reaction mechanism, energy transfer, and energy dissipation with the help of the RPH.

2.2 Methods to Locate Stationary Points on the PES

2.2.1 Definition of Stationary Points

The important regions of the PES are those which harbour minima and first order saddlepoints. Minima correspond to the *equilibrium geometries* of reactants, products, and possible stable intermediates of a chemical reaction. A saddlepoint of first order is the highest energy point on the *minimum energy path* connecting two minima.[14] It is the mountain pass

connecting the reactant valley to the product valley, which must be surmounted before the chemical reaction can take place (ignoring tunneling, of course). Both minima and first order saddlepoints are stationary or critical points (chemists prefer to use the former term). At the stationary points, the gradient of $V(\boldsymbol{R})$ vanishes, i.e., all elements of the gradient expressed in internal coordinates are zero:

$$g_k = \frac{\partial V(\boldsymbol{R})}{\partial R_k} = 0 \quad k = 1, 2, \ldots, 3K - L \tag{1}$$

Since the elements of the gradient correspond to the forces exerted on the nuclei, stationary points are characterized by the fact that there are no internal forces on the atoms. The nature of a given stationary point can be described by the *Hessian matrix*, i.e., the matrix of second derivatives of the energy, which defines the force constant matrix $\mathbf{F}$ with elements

$$F_{kl} = \frac{\partial^2 V(\boldsymbol{R})}{\partial R_k \partial R_l} \tag{2}$$

At a minimum, the eigenvalues of $\mathbf{F}$ are all positive ($3K - L$ positive curvatures λ_i, matrix $\mathbf{F}$ is positive definite; see Table 1), which means that at this point the PES is curved in all directions concavely upward. For first-order saddlepoints there is one and only one negative eigenvalue of $\mathbf{F}$. In this case, the PES is a minimum in $(3K - L - 1)$ dimensions while in the remaining dimension it is a maximum. Since the PES is a smooth, contiguous function connecting all its minima, there must be at least one first-order saddlepoint between two connected minima. For a PES with n minima, there are indeed $(n - 1)$ first-order saddlepoints.[15,16]

Other stationary points on the PES may correspond to higher-order saddlepoints with $2, \ldots, n$ negative eigenvalues of $\mathbf{F}$ or even to maxima with all eigenvalues being negative. However, these stationary points are chemically not relevant since it is always possible for a reaction system to find a lower energy path that passes through a first-order rather than any higher-order saddlepoint.[14]

2.2.2 *Location of Stationary Points: Geometry Optimization*

A series of mathematical algorithms is now available to locate stationary points on the PES (see ***Geometry Optimization: 1*** and ***Geometry Optimization: 2***).[17–19] These can be grouped into methods that use (a) just the energy, (b) energy and *energy gradient*, or (c) energy, energy gradient, and Hessian matrix of the energy. Energy-only methods are the least costly ones, however search strategies for stationary points based on energy-only methods often converge rather slowly and, therefore, they are seldom used for determining the minima and saddlepoints on an *ab initio* PES. Because of the availability of analytical first and often also second energy derivatives for HF-based and correlation-corrected *ab initio* methods,[20,21] gradient (first derivative), Newton (second derivatives), or combination methods are nowadays preferably used for the location of stationary points.[17–19]

Table 1 Stationary Points on a Potential Energy Surface $V(\boldsymbol{R})$

Stationary point	Curvature λ	Location of
Minimum	$\lambda_i > 0$ for $i = 1, \ldots, 3K - L$	Reactant or Product
Saddlepoint of first order	$\lambda_1 < 0; \lambda_i > 0$ for $i = 2, \ldots, 3K - L$	Transition State
Saddlepoint of higher order $n > 1$	$\lambda_i < 0$ for $i = 1, \ldots, n$ $\lambda_i > 0$ for $i = n + 1, \ldots, 3K - L$	(chemically not relevant)
Maximum	$\lambda_i < 0$ for $i = 1, \ldots, 3K - L$	

One of the most cited representatives of the Newton methods is the Newton–Raphson approach,[22] for which the PES function $V(\boldsymbol{R})$ is expanded at a point $\boldsymbol{R}_0$ close to the stationary point $\boldsymbol{R}_{sp}$ by a Taylor series expansion:

$$V(\boldsymbol{R}) = V_0(\boldsymbol{R}) + \sum_k^{3K-L} g_k(\boldsymbol{R}_0)\Delta R_k + \frac{1}{2}\sum_{k,l}^{3K-L} F_{kl}(\boldsymbol{R}_0)\Delta R_k \Delta R_l \tag{3a}$$

$$V(\boldsymbol{R}) = V_0(\boldsymbol{R}) + \boldsymbol{g}^+ \Delta \boldsymbol{R} + \frac{1}{2}\Delta \boldsymbol{R}^+ \boldsymbol{F} \Delta \boldsymbol{R} \tag{3b}$$

with $$\Delta R_k = R_k - R_{0,k} \tag{4}$$

and the expansion being truncated at the second-order terms. At a stationary point, condition (1) must be satisfied. Hence, the Newton–Raphson step to be taken to get from the current point to the stationary point is given by equation (5):

$$\Delta \boldsymbol{R} = \boldsymbol{R}_{new} - \boldsymbol{R}_0 = -\boldsymbol{F}^{-1}\boldsymbol{g} \tag{5}$$

where $\boldsymbol{R}_{new}$ is the new point reached by carrying out (5). If $V(\boldsymbol{R})$ is quadratic in the region containing $\boldsymbol{R}_0$ and $\boldsymbol{R}_{sp}$, the new point will be identical to the stationary point. Since this is usually not the case, an iterative procedure is required to find $\boldsymbol{R}_{sp}$. To determine if the point $\boldsymbol{R}_{new}$ predicted by equation (5) is a stationary point, $\boldsymbol{g}(\boldsymbol{R}_{new})$ will be computed. If $|\boldsymbol{g}(\boldsymbol{R}_{new})|$ is larger than a given threshold ε, equation (5) will be re-evaluated until $|\boldsymbol{g}(\boldsymbol{R}_{new})| \leq \varepsilon$. To make the search for $\boldsymbol{R}_{sp}$ more efficient, the length of the correction vector $\Delta \boldsymbol{R}$ is adjusted by determining the point along $\Delta \boldsymbol{R}$ for which the energy of the gradient length $\|\boldsymbol{g}\|$ is a minimum[23], i.e., an optimal parameter α is introduced to minimize $E(\boldsymbol{R}_0 + \alpha \Delta \boldsymbol{R})$ or $\|\boldsymbol{g}(\boldsymbol{R}_0 + \alpha \Delta \boldsymbol{R})\|$. This procedure ensures that the new point is the optimum point along the correction vector for the next iteration.

Since the cost of computing second derivatives is substantially higher than the cost of computing energy and gradient, one uses quasi-Newton algorithms for which the Hessian is not explicitly computed during the iterative search for a stationary point.[23] Accordingly, quasi-Newton methods take an intermediate position between gradient and Newton methods. Their cost requirements are comparable to gradient methods, however their performance approaches that of the Newton–Raphson method.[23] In the case of a quasi-Newton method, an initial Hessian matrix is updated in each search step utilizing the computed changes in the gradient. Quasi-Newton methods differ by the initial guess for the *Hessian* (force constant) *matrix* $\mathbf{F}$, which may be the unit matrix or an estimated force constant matrix, and the manner in which the Hessian or its inverse is updated during the course of the *optimization*.[18,19,23]

While it is possible to find starting geometries for equilibrium optimizations of most reactants and products that are

within or at least in the vicinity of the quadratically convergent region so that Newton or quasi-Newton methods rapidly lead to the corresponding minimum, this is often no longer true in the case of saddlepoint geometries. For a given starting point in a TS search, the local Hessian matrix may not have the correct structure leading to $(3K - L - 1)$ positive and one negative eigenvalue. In this case, a step must be chosen in a direction leading to the TS region. To solve this problem, a quasi-Newton-like algorithm has been proposed by Simons and co-workers[24,25] and improved by Baker[26], which follows that mode that leads to the TS in question (mode-following[27]). For this purpose, one assumes that the mode with the lowest eigenvalue λ_n leads uphill toward the saddlepoint. If λ_n happens to be positive, a shift parameter Δ is calculated so that $\lambda_n - \Delta$ becomes negative while the corresponding differences for all other eigenvalues are still positive so that in these directions a minimum optimization can still be performed.

Due to the availability of effective search methods, the localization of stationary points on the PES has become routine. Nevertheless, in particularly difficult cases further refinements of available algorithms may be needed.

2.3 Reaction Path and Reaction Path Following Methods

2.3.1 *Definition of the Reaction Path: The Steepest Descent Path*

In the literature, the term reaction path is interchangeably used with terms such as 'reaction coordinate', 'steepest descent path', 'path of least energy', 'minimum energy path', etc.[19,28–30] Apart from this, the definition of a RP is often confused by mixing it with ill-defined concepts such as the distinguished reaction coordinate (see Figure 1). Even today, many textbooks discuss the mechanism and the dynamics of chemical reactions assuming that one of the internal coordinates of the reaction complex varies monotonically from reactants to products and, therefore, is best suited as a distinguished reaction coordinate. This assumption suffers from the fact that it is not always possible to relate an appropriate reaction coordinate to one of the internal coordinates. Furthermore, if a distinguished reaction coordinate can be chosen, there will be no guarantee that the RP passes through the first-order saddlepoint and, thereby, defines the lowest energy barrier separating reactants from products. Finally, the other internal coordinates may depend discontinuously on the distinguished reaction coordinate because of strong coupling between the internal coordinates and an arbitrarily chosen reaction coordinate.

A more objective way to define the RP is to start at the first order saddlepoint separating reactants from products and to follow the steepest descent path in one direction to reactants and in the other direction to products as was first suggested by Fukui[5] although the concept appears to have a long history. The steepest descent path follows the gradient of the PES function $V(\boldsymbol{R})$. It is the path that molasses would follow flowing downhill. One can show by expanding $V(\boldsymbol{R})$ to first order at a given point of the path that for the steepest descent path the length of the step in any given internal coordinate is proportional to the negative of the gradient of the energy in that direction:

$$\Delta R_k = -\alpha g_k \tag{6}$$

where α is a proportionality constant that defines an optimal step length along the path. Equation (6) is no longer true at the first order saddlepoint since the gradient vanishes at this point. In this case, one has to expand $V(\boldsymbol{R})$ to second order to show that the direction of the steepest descent path is given by the eigenvector associated with the negative eigenvalue of the Hessian matrix. Hence, the steepest descent path passes continuously from reactants to products through the saddlepoint.[31]

Although the steepest descent path traces out a reasonable RP, it is first of all just a mathematical recipe that cannot necessarily be used to describe the dynamics of a chemical reaction. Its major flaw is that, contrary to the stationary points, it depends on the choice of the coordinate system and, in this respect, does not represent a unique path.[32]

2.3.2 *Definition of the Reaction Path: The Intrinsic Reaction Path*

The dynamics of a reaction complex is connected with the intrinsic reaction coordinate (IRC) or, better, intrinsic reaction path (IRC path), which is simply the steepest descent path expressed in mass-weighted Cartesian coordinates. The IRC path was first used by Eliason and Hirschfelder[33], and later investigated in great detail by Fukui and co-workers.[34]

The necessity of mass scaling can be explained by the example of two noninteracting H_2 molecules at their equilibrium geometries.[19] For small deviations from the equilibrium geometry, a contour line diagram of the corresponding PES expressed in terms of the two displacement coordinates X_1 and X_2 (Figure 2a) is given by a series of concentric circles, which indicate that the function $V(X_1, X_2)$ increases in all directions uniformly upon stretching $(X_{1,2} > 0)$ or compressing $(X_{1,2} < 0)$ the H–H bond lengths. When the two H–H bond lengths are stretched by the same amount $X_1 = X_2$, the potential energy V increases by an amount $\Delta V = V(X_1, X_2) - V_0$ (Figure 2a). Upon relaxing the molecules, a force acts on the system in the direction of the negative of the gradient vector and ΔV is converted into kinetic energy. To understand the dynamics of the system, it may be compared with a frictionless billiard ball rolling down the slope of the PES. At point (X_1, X_2), the acceleration $\ddot{\boldsymbol{X}}$ of the ball can be calculated from

$$m\ddot{\boldsymbol{X}} + k\boldsymbol{X} = 0 \tag{7a}$$

$$\ddot{\boldsymbol{X}} = -\frac{k\boldsymbol{X}}{m} \tag{7b}$$

(k: force constant, m: mass; harmonic approximation; zero velocity at point (X_1, X_2)). It depends on the masses; however, since the masses of the two subsystems are identical, the acceleration is parallel to the force (Figure 2a) and the frictionless ball will roll back and forth with its trajectory being perpendicular to the contour lines and passing through the equilibrium point.

The situation will be different if the second H_2 molecule is replaced by D_2. Although the form of the PES does not change since it is independent of the masses of isotopomers (Figure 2b), the dynamics of the rolling ball does. At point (X_1, X_2), the component of the acceleration vector in the X_2 direction is half as large as the one in the X_1 direction since the corresponding mass has doubled. Applied force and acceleration are no longer parallel, which means that the initial movement of the ball is no longer directed toward the equilibrium point and is no longer perpendicular to the contour lines. Physically this does not make sense since the ball should still take the shortest path to the equilibrium point and this

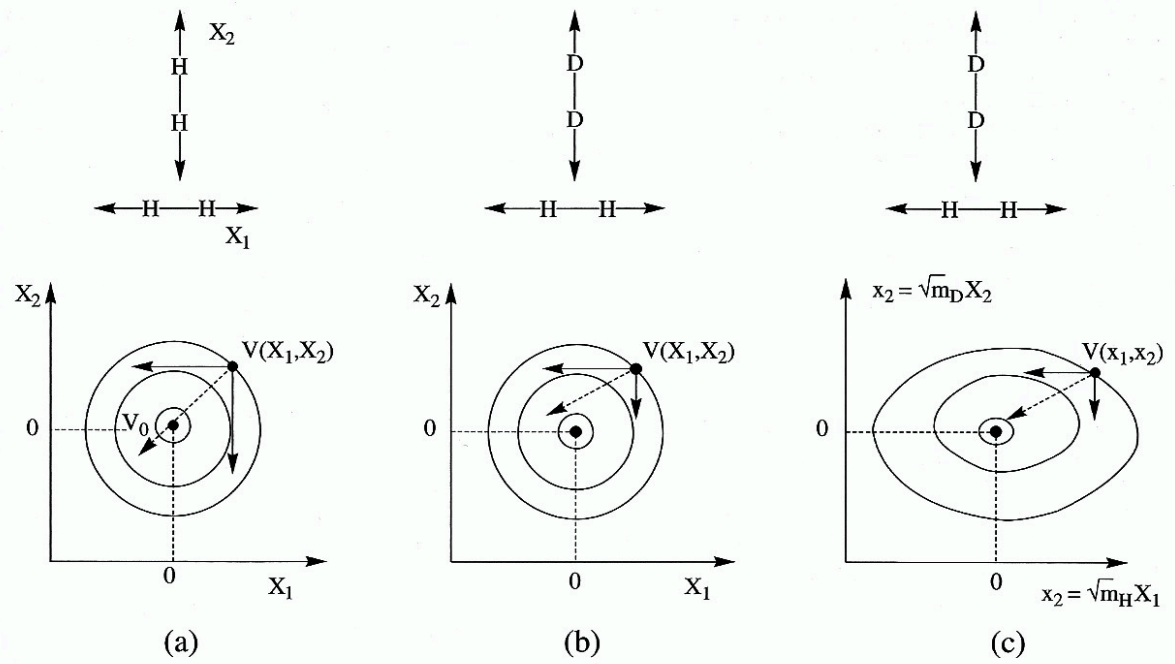

Figure 2 Contour line diagrams of the potential V for the system of two noninteracting molecules: (a) $V(X_1, X_2)$ for $H_2 \cdots H_2$; (b) $V(X_1, X_2)$ for $H_2 \cdots D_2$; (c) $V(x_1, x_2)$ for $H_2 \cdots D_2$. X and x denote normal and mass-weighted Cartesian displacement coordinates, respectively. The components of the acceleration vector are given at point (X_1, X_2)

path should be independent of the coordinates used. To fulfil this prerequisite, the PES is expressed in a mass-weighted coordinate system where both X_1 and X_2 are multiplied with the square root of the corresponding mass:

$$x_1 = \sqrt{m_1} X_1 \tag{8a}$$

$$x_2 = \sqrt{m_2} X_2 \tag{8b}$$

By this transformation the contour lines of the PES are elongated (Figure 2c) even though the potential energy $V(X_1, X_2)$ has still the same form for the two isotopomers. The acceleration vector is once again parallel to the applied force and the ball will roll directly toward the minimum, i.e., the dynamics of the $H_2 \cdots H_2$ system is restored. The ball follows the IRC path.

In more general terms, the connection between IRC path and reaction dynamics can be made clear when considering the classical equations of motion for nuclei moving on the PES:[35]

$$\frac{\mathrm{d}}{\mathrm{d}t}(m_i \dot{X}_i) = -\frac{\partial V(\boldsymbol{X})}{\partial X_i} = -g_i \quad (i = 1, 2, 3, \ldots 3K) \tag{9}$$

where X_i denote the Cartesian coordinates of the nuclei of the reaction complex. Assuming that the nuclei move down the path from the TS toward either reactant or product minimum with an infinitesimal velocity, equation (9) can be integrated to yield:

$$m_i \dot{X}_i = -\frac{\partial V(\boldsymbol{X})}{\partial X_i} t = -g_i t \tag{10}$$

The set of equations (11) is obtained:

$$\frac{m_1 \mathrm{d}X_1}{\dfrac{\partial V(\boldsymbol{X})}{\partial X_1}} = \frac{m_2 \mathrm{d}X_2}{\dfrac{\partial V(\boldsymbol{X})}{\partial X_2}} = \frac{m_3 \mathrm{d}X_3}{\dfrac{\partial V(\boldsymbol{X})}{\partial X_3}} = \cdots \tag{11}$$

which by introducing mass-weighted Cartesian coordinates gives:

$$\frac{\mathrm{d}x_1}{\dfrac{\partial V(\boldsymbol{x})}{\partial x_1}} = \frac{\mathrm{d}x_2}{\dfrac{\partial V(\boldsymbol{x})}{\partial x_2}} = \frac{\mathrm{d}x_2}{\dfrac{\partial V(\boldsymbol{x})}{\partial x_2}} = \cdots \tag{12a}$$

$$\frac{\mathrm{d}x_1}{g_1} = \frac{\mathrm{d}x_2}{g_2} = \frac{\mathrm{d}x_3}{g_3} = \cdots \tag{12b}$$

Since the gradient of $V(\boldsymbol{R})$ is proportional to the force acting on the atoms, equation (12) implies that the changes in the mass-weighted coordinate x_i are proportional to the force in the direction of x_i. The larger the force in this direction, the longer the displacement in this direction is. The IRC path corresponds to the classical trajectory obtained by starting at the saddlepoint and moving with a constantly damped velocity toward either the reactants or the products. Since the classical equations of motion are independent of the choice of the coordinate system, the IRC path is uniquely defined.

Although the use of $3K$ Cartesian coordinates to calculate the IRC path for a K-atomic reaction complex is straightforward, Cartesian coordinates are not suitable for representing the PES since the function $V(\boldsymbol{R})$ does not depend on the L overall translations and rotations of the reaction complex and, accordingly, is only a function of $(3K - L)$ internal coordinates. To describe the motion of the nuclei on the PES, one has to back-transform from the $3K$ Cartesian coordinates $\{X_i\}$ to $(3K - L)$ internal coordinates $\{R_k\}$ where the three translations and three rotations are eliminated by the center of mass and Eckart conditions.[36] However, the space in which the internal motions are separated from translations and rotations is Riemanian rather than Euclidean.[37] One has to define an appropriate matrix in this space by the tensor elements $a_{k,l}$:

$$a_{k,l} = \sum_i m_i \left(\frac{\partial X_i}{\partial R_k}\right)\left(\frac{\partial X_i}{\partial R_l}\right) \tag{13}$$

and, then, to express the IRC equation in terms of internal coordinates $\{R_k\}$:

$$\sum_k a_{1,k}\left(\frac{\partial R_1}{\partial g_1}\right) = \sum_k a_{2,k}\left(\frac{\partial R_2}{\partial g_2}\right) = \cdots \tag{14}$$

The elements $a^{-1}_{k,l}$ of the inverse matrix are given by

$$a^{-1}_{k,l} = G_{k,l} = \sum_i^{3K} \frac{1}{m_i} B_{k,i} B_{l,i} = \sum_i^{3K} \frac{1}{m_i}\left(\frac{\partial R_k}{\partial X_i}\right)\left(\frac{\partial R_l}{\partial X_i}\right) \tag{15}$$

where $G_{k,l}$ and $B_{k,i}$ are elements of Wilson's **G** and **B** matrices, respectively.[38] For all sets of internal coordinates $\{R_k\}$ derived from $3K$ Cartesian coordinates by the use of equation (12), solution of equation (14) will yield the same IRC path.

Fukui and co-workers[39] showed that the IRC path is the shortest path from a minimum to the saddlepoint with the length being equal to the barrier height. Igawa and Fukutome[40] showed that the IRC path corresponds to the least motion path, which is the most favorable RP according to the principle of least motion in chemical reactions.[41] Since the IRC path is uniquely defined, mathematically rigorous, and conceptually appealing, it is the appropriate path to investigate reaction mechanism and reaction dynamics.

2.3.3 *Reaction Path Following Methods*

The RP can be represented as a Taylor series in s expanded about $\boldsymbol{x}_S(s_0)$ for any point $\boldsymbol{x}_S(s_0)$ on the RP (except at the saddlepoint)[19,42]

$$\boldsymbol{x}_S(s) = \boldsymbol{x}_S(s_0) + c_S^{(1)}(S - S_0) + \frac{1}{2!}c_S^{(2)}(S - S_0)^2 + \cdots + \frac{1}{n!}c_S^{(n)}(S - S_0)^n \tag{16}$$

where the expansion coefficients $c_S^{(i)}$ depend only on the energy derivatives evaluated at $\boldsymbol{x}_S(s_0)$. The reaction coordinate vector $\boldsymbol{x}_S(s)$ depends parametrically on the path length s, which is defined as the mass-weighted Cartesian distance along the path

$$ds^2 = \sum_i dx_i^2 \tag{17}$$

The first two coefficients in expansion (16) correspond to the normalized reaction path vector (path tangent) $\boldsymbol{t}(s)$ and the reaction path curvature vector $\boldsymbol{k}(s)$ (see Figure 3):

$$c_S^{(1)}(s) = \frac{d\boldsymbol{x}_S(s)}{ds} = -\frac{\mathbf{g}^x(s)}{\|\mathbf{g}^x(s)\|} = \boldsymbol{t}(s) \tag{18a}$$

$$\|\boldsymbol{g}^x(s)\| = [\boldsymbol{g}(s)^+\mathbf{M}^{-1}\boldsymbol{g}(s)]^{1/2} \tag{18b}$$

$$c_S^{(2)}(s) = \frac{d\boldsymbol{t}(s)}{ds} = \frac{d^2\boldsymbol{x}_S(s)}{ds^2} = \boldsymbol{k}(s) \tag{19a}$$

$$\boldsymbol{k}(s) = \|\boldsymbol{k}(s)\| = [\boldsymbol{k}(s)^+\boldsymbol{k}(s)]^{1/2} \tag{19b}$$

where the superscript x denotes mass-weighting and the Euclidian norm of gradient and curvature vector are also given. The curvature vector corresponds to the principal normal vector of the RP curve and is directed toward the concave side of the RP. It is obtained by differentiating equation (19a) with respect to s by use of the chain rule (gradient $\boldsymbol{g}^x$ depends on s only implicitly through its dependence on $\boldsymbol{x}_S$) :

$$\boldsymbol{k}(s) = \frac{1}{\|\boldsymbol{g}^x(s)\|}[\mathbf{F}^x(s)\boldsymbol{t}(s) - \{\boldsymbol{t}(s)^+\mathbf{F}^x(s)\boldsymbol{t}(s)\}\boldsymbol{t}(s)] \tag{20}$$

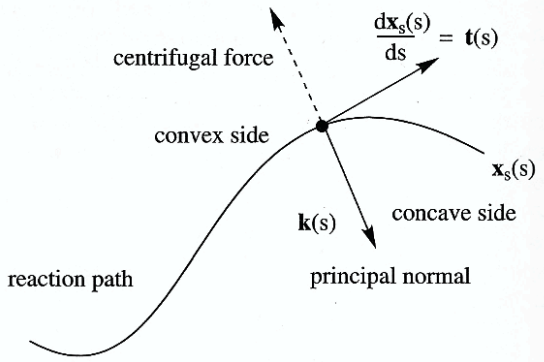

Figure 3 Schematic representation of reaction path vector $\boldsymbol{t}(s)$ and curvature vector $\boldsymbol{k}(s)$ at a point s of a curved reaction path $\boldsymbol{x}_S(s)$

Formulae for higher derivatives $c^{(n)}(s)$ have been given by Page and McIver[42] and Gonzales and Schlegel (see ***Reaction Path Following***).[43]

The number of terms included in expansion (16) strongly affects the stability and effectiveness of the algorithms for calculating a RP. The simplest and hence most commonly used methods are the Euler methods, which neglect all terms in equation (16) higher than first order. So-called Euler single step methods use only the energy gradient at a given s_m to predict the next point $\boldsymbol{x}_S(s_{m+1})$ of the path:

$$\boldsymbol{x}_S(s_{m+1}) = \boldsymbol{x}_S(s_m) - \Delta s\boldsymbol{t}(s) \tag{21}$$

where Δs is the step size. Gradient-following methods often trace out an approximate RP that meanders ('oscillates') around the true path. One can avoid these oscillations by using very small step sizes or applying a stiff differential equation solver.[29] Alternatively, an Euler stabilization method[44] can be employed, in which the Euler single step (predictor step) is combined with a corrector step. For example, Ishida, Morokuma, and Komornicki[45] added a one-dimensional search step along the bisector of the old and new gradient to damp out oscillations of the Euler single step.[46]

Since all Euler methods neglect the curvature term in equation (16), they are not suited for the description of strongly curved paths. A method suggested by Gonzales and Schlegel[47] addresses this deficiency by choosing the new point s_{m+1} so that the approximate path between s_m and s_{m+1} is the arc of a circle and the gradient vectors $\boldsymbol{g}(s_m)$ and $\boldsymbol{g}(s_{m+1})$ are tangents to this approximate path. If the two tangents to the circle intersect at point s^*_{m+1}, the three points s_m, s^*_{m+1}, and s_{m+1} form an isosceles triangle. The pivot point s^*_{m+1} is found by first taking a step of length $\Delta s/2$ along gradient $\boldsymbol{g}(s_m)$. At point s^*_{m+1} a constrained optimization is carried out on the surface of a sphere of radius $\Delta s/2$ and centred at s^*_{m+1} leading to s_{m+1} using second derivative information (either exact or approximate).

Page and McIver[42] proposed an *algorithm* which takes the curvature term of equation (16) into account and, accordingly, leads to a local quadratic approximation of the RP at s_m. In this way, a RP can be determined which has the correct curvature at the point of expansion. Special efforts have to be taken to determine the direction and curvature of the RP at the saddlepoint. Since the gradient vanishes at this point, second and third energy derivatives (Hessian and first derivatives of the Hessian), have to be calculated according to the rule of L'Hospital.[42] Hence, the local quadratic approximation of Page

and McIver[42] is more reliable at the saddlepoint and in all those regions where the RP is strongly curved.[44]

Most computational investigations of the IRC path use mass-weighted internal coordinates rather than Cartesian coordinates. This is done by directly solving the equations of motion in internal coordinates $\{r_k\}$ using the Wilson **G** matrix:[47]

$$\frac{\mathrm{d}}{\mathrm{d}t}\left(\frac{\partial T}{\partial \dot{\boldsymbol{r}}}\right) + \left(\frac{\partial V(\boldsymbol{r})}{\partial \boldsymbol{r}}\right) = 0 \tag{22}$$

where the kinetic energy T is given by

$$T = \tfrac{1}{2}\dot{\mathbf{R}}^{+}\mathbf{G}^{-1}\dot{\mathbf{R}} = \tfrac{1}{2}\dot{\boldsymbol{r}}^{+}\boldsymbol{r} \tag{23}$$

In this way, the IRC path in terms of mass-weighted internal coordinates $\boldsymbol{r}$ is obtained:

$$\frac{\mathrm{d}\boldsymbol{r}_s(s)}{\mathrm{d}s} = -\frac{\mathbf{G}_g}{[\boldsymbol{g}^{+}\mathbf{G}\boldsymbol{g}]^{1/2}} \tag{24}$$

in analogy to equation (18a), i.e., the IRC path of equation (24) is identical to the IRC path in mass-weighted Cartesian coordinates $\boldsymbol{x}$.

2.3.4 *Bifurcating Reaction Paths*

The energy gradient, which determines the direction of the RP, transforms according to the totally symmetric irreducible representation of the symmetry of the reaction complex.[48] The intrinsic RP is also totally symmetric so that the reaction complex never loses its symmetry along the RP. Exceptions in this respect are the stationary points (minima, first-order saddlepoints) where other than totally symmetric directions can be taken by the reaction complex.

Yet another exception is encountered at unstable path points.[49] Suppose one walks down the path and the $(3K - L - 1)$-dimensional reaction valley becomes flatter and flatter in one direction, i.e., one eigenvalue of the Hessian matrix decreases to zero.[50,51] At the point for which the eigenvalue is identical to zero, the path becomes unstable and bifurcates into two new paths. Following one of the two new RPs leads to a lowering of the symmetry of the reaction complex. However, when enforcing the original symmetry of the reaction complex, the latter follows a ridge path between the two new reaction valleys where the ridge path is unstable with regard to any lateral displacement in the direction of the eigenvector corresponding to the negative eigenvalue of the Hessian (force constant) matrix.

Branching or *bifurcation points* can occur in all regions along the RP. Three different situations can be distinguished (Figure 4):[51] (a) The RP can split and merge again somewhere in the entrance or exit channel. The original path traces out a local energy ridge that is avoided (unstable region) by the two new paths. (b) There is the possibility that a chemically reasonable RP turns out to be unstable in the TS region. Then there are two paths of lower energy that avoid the original TS, which in this case turns out to be a second-order rather than a first-order saddlepoint. (c) Frequently, the RP splits in the exit channel into two new RP, which lead to two rather than one product minimum. There is a third path that combines one product minimum with the other via a new first-order saddlepoint, which corresponds to the minimum of the ridge path between the new RPs.

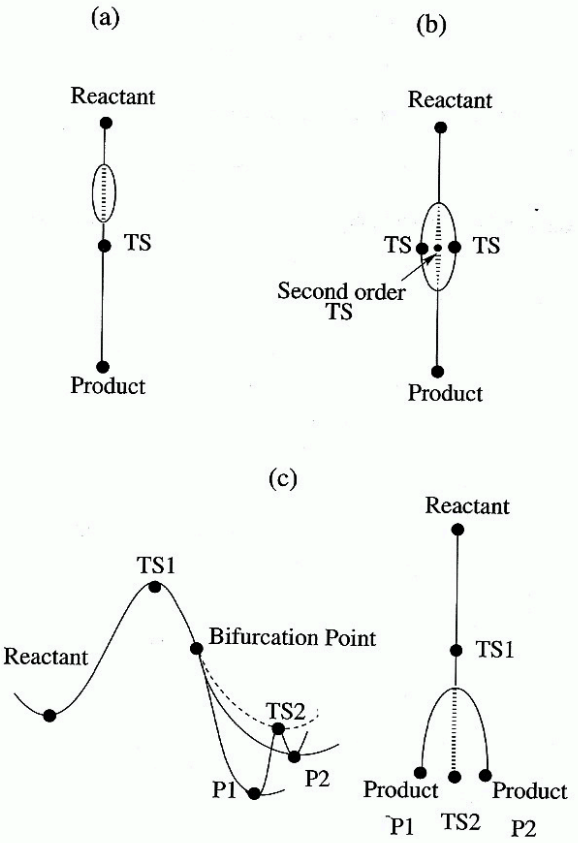

Figure 4 Schematic representation of three types of unstable RP regions (denoted by a hashed line) with bifurcation points: (a) the unstable region is located between TS and reactant (or product) minimum; (b) the unstable region contains a second order saddlepoint; (c) the unstable region coincides with the product (or reactant) region

Besides single bifurcations, there is also the possibility of triple bifurcations (two eigenvalues of the Hessian become zero) and even higher bifurcations. In principle, it is not difficult to detect bifurcation points and algorithms have been proposed to determine the location of a bifurcation point.[50,51] However, it is somewhat more difficult to correctly follow a bifurcating path.

Bifurcating RPs, in particular of type (a) (Figure 4), often indicate a deficiency of the quantum chemical method used to describe the RP. Therefore, their chemical relevance has to be checked by higher level methods. In particular, if a RP is investigated that has been obtained by some scaling or fitting procedure, it will have to be checked whether bifurcations of the RP are not simply a result of discontinuities in the scaling procedure. However, if they are real, they will complicate dynamic studies. Bifurcating RPs mostly indicate the possibility of LAMs, which explicitly have to be included in a dynamic model of the chemical reaction.

2.4 The Reaction Valley and the Reaction Path Hamiltonian

2.4.1 *Description of the Reaction Valley*

To explore mechanism and dynamics of a chemical reaction to a larger extent, the immediate vicinity of the RP on the PES is included in the description. This can be done by considering

the one-dimensional RP and the $(3K-L-1)$ (in the general case: $3K-7$) directions orthogonal to the RP. Since the IRC path defines the points of minimum energy a movement in any direction orthogonal to the IRC path leads to an increase in energy, i.e., one has to climb up the 'energy walls' of a valley on the PES. Accordingly, one can speak of a $(3K-L-1)$-dimensional reaction valley leading from reactants through the saddlepoint to the products.

To describe the reaction valley an appropriate set of coordinates is needed, where one of the coordinates describes the motion along the path and the other coordinates describe the transverse motions. Such coordinates have been termed natural reaction coordinates. The idea of characterizing a reacting system by natural coordinates has emerged out of early work of Hofacker (1963)[52], in particular Marcus (1966)[53] (natural collision coordinates that define a RP as a curve where the classical local vibrational and internal centrifugal forces balance), and others.[54,55] Also influential was the work by Hougen, Bunker, and Johns,[56] who developed a model for treating the LAMs which are frequently observed in vibrational–rotational spectroscopy, apart from all the other internal coordinates.

In 1980, Miller, Handy, and Adams[4] derived a classical Hamiltonian for a reacting molecular system, which combined the early ideas of Hofacker and Marcus, the IRC path of Fukui, and the large amplitude model of Hougen, Bunker, and Johns. Essential to their derivation was the idea of a reaction valley as the scene of all mechanistic and dynamic steps accompanying a chemical reaction. The valley can be compared with a stream bed with $(3K-L-1)$ harmonic walls that are free to close in or to widen out as one proceeds along the stream bed. Miller, Handy, and Adams described the reacting system in terms of a RP coordinate set being composed of the reaction coordinate s and $(3K-L-1)$ complementary reaction valley coordinates. In principal, one could use for the latter internal coordinates; however, these define directions not necessarily orthogonal to the path. Clearly, the reaction valley can better be described by determining at each path point s the curvature of the valley floor in directions perpendicular to the RP. This can be done by considering that for a fixed value of s the potential energy $V(\boldsymbol{R})$ is a minimum in the $(3K-L-1)$-dimensional subspace orthogonal to the RP subspace. Expanding $V(\boldsymbol{R})$ up to second order, the curvatures of the valley and, by this, its steepness can be calculated in the same way as is done for a minimum in the full space. The only difference is that the Hessian (force constant) matrix at point s is expressed in mass-weighted coordinates and constructed by projecting out not only rotations and translations of the reaction complex but also its translational motion along the RP thus yielding the mass-weighted projected force constant matrix $\mathbf{K}(s)$:

$$\mathbf{K}(s) = [\mathbf{I} - \mathbf{P}(s)]^{+}\mathbf{F}^{x}(s)[\mathbf{I} - \mathbf{P}(s)] \tag{25}$$

where $(\mathbf{I} - \mathbf{P}(s))$ is a projection onto the $(3K-L-1)$-dimensional subspace. By diagonalizing, i.e., solving the vibrational eigenvalue equation (26):

$$\mathbf{K}(s)\boldsymbol{l}_{\mu}(s) = \omega_{\mu}^{2}(s)\boldsymbol{l}_{\mu}(s) \tag{26}$$

$(3K-L-1)$ mass-weighted generalized normal modes $\boldsymbol{l}_{\mu}(s)$ and their associated frequencies $\omega_{\mu}(s)$ are obtained while $L+1$ frequencies corresponding to translations, rotations, and the motion along the RP are set equal to zero. The generalized normal mode vectors are orthogonal to the RP and span the $(3K-L-1)$-dimensional subspace of the reaction valley. Hence, the normal mode coordinates $Q_{\mu}(s)$ are perfectly suited for the description of the valley. The frequencies $\omega_{\mu}(s)$ describe the curvature and the steepness of the valley walls in the $(3K-L-1)$ directions. Large frequencies indicate steep energy walls while small frequencies describe a flat valley with only slowly increasing energy walls. One speaks of a harmonic reaction valley since the potential energy V is expanded in this description just to second order. Each point $\boldsymbol{x}_i$ in mass-weighted Cartesian coordinate space is given by

$$\boldsymbol{x}_i = \boldsymbol{x}_i(s) + \sum_{\mu}^{3K-L-1} \boldsymbol{l}_{\mu,i}(s)Q_{\mu} \tag{27}$$

i.e., as a linear combination of the path coordinate and the orthogonal valley coordinates.

2.4.2 *The Reaction Path Hamiltonian of Miller, Handy, and Adams*

The original RPH of Miller, Handy, and Adams[4] is a classical Hamiltonian that is formulated considering a number of assumptions.

(1) The first one is the assumption of a harmonic reaction valley, which can be fully described with the help of the mass-weighted projected force constant matrix $\mathbf{K}(s)$ evaluated at each path point of interest.

(2) As a consequence of the harmonic expansion of the valley potential, just the kinetic part, but not the potential energy part of the RPH contains the coupling terms between different vibrational modes. Hence, the RPH is an adiabatic Hamiltonian and a consequence of the adiabaticity of the RPH is that the frequencies $\omega_{\mu}(s)$ of generalized normal modes with the same symmetry must not cross.

(3) To further simplify the RPH, rotations of the reaction complex in three-dimensional space are excluded by assuming zero angular momentum ($\mathbf{J} = 0$). In this way, the RPH does not contain a rotational part and possible rotational–vibrational coupling terms.

(4) In addition, one assumes that the movement along the RP is very slow compared to the transverse vibrational motions (vibrationally adiabatic assumption). In this way, it is guaranteed that all transverse vibrational modes stay in the same eigenstate throughout the whole reaction, i.e., one can focus just on the vibrational ground states of the transverse normal modes and calculate on this basis a vibrationally adiabatic potential that reflects the influence of the transverse vibrations on the energy profile along the RP.

With these assumptions, the RPH adopts the form of equation (28):[4]

$$H[s, p_s, \{Q_{\mu}\}\{P_{\mu}\}] = T[s, p_s, \{Q_{\mu}\}\{P_{\mu}\}] + V[s\{Q_{\mu}\}] \tag{28a}$$

where $(s, \{Q_{\mu}\})$ are the reaction valley coordinates and $(p_s, \{P_{\mu}\})$ denote their conjugated momenta. The potential V is approximated at each point s by the potential V_0 at s plus the potential for harmonic displacements perpendicular to the

path:

$$V[s, \{Q_\mu\}] = V_0(s) + \frac{1}{2}\sum_{\mu}^{3K-L-1} \omega_\mu^2(s)\, Q_\mu^2(s) \tag{28b}$$

The kinetic energy is given by (for zero total angular momentum):

$$T[s, p_s, \{Q_\mu\}\{P_\mu\}] = \frac{1}{2}\frac{\left[p_s - \sum_{\mu}^{3K-L-1}\sum_{\nu} B_{\mu,\nu}(s) Q_\mu(s) P_\nu(s)\right]^2}{\left[1 + \sum_{\mu}^{3K-L-1} B_{\mu,s}(s)\, Q_\mu(s)\right]^2} + \frac{1}{2}\sum_{\mu}^{3K-L-1} P_\mu^2(s) \tag{29}$$

The first term corresponds to the kinetic energy part of the movement along the RP including coupling terms between RP and transverse motions. The second term represents the kinetic energy part associated with a movement orthogonal to the path direction. The numerator of the first term is the generalized momentum of the RP motion and the denominator represents an effective mass μ_{eff}, which is of relevance for tunneling investigations. The direction of the mode vector $\boldsymbol{l}_\mu(s)$ at s is chosen in such a way that the product $Q_\mu(s)B_{\mu,s}(s)$ becomes negative when $Q_\mu(s)$ is taken on the concave side of the RP (Figure 3). Hence, curvature of the RP lowers the effective mass and, accordingly, raises the tunneling probability.[57] If the sum in the denominator of the first term becomes smaller than -1 in the case of large curvature, $(\mu_{\text{eff}})^{1/2} < 0$ will indicate that the coordinate system of the RP is no longer suitable and that the concept of the RPH has to be extended by including those modes that are responsible for the large curvature couplings.

2.4.3 *Mechanistic and Dynamic Information Provided by the RPH*

There are two different types of terms in the RPH which explicitly depend on the PES:

(a) Shape terms $\boldsymbol{x}_s(s)$, $V_0(s)$, and $\{\omega_\mu(s)\}$: The shape of the reaction valley leading from reactants over the barrier to products is characterized by the reaction coordinate vector $\boldsymbol{x}_s(s)$, which determines the meandering of the floor line of the reaction valley, the classical potential energy $V_0(s)$, which determines the height of the path, and the vibrational frequencies $\{\omega_\mu(s)\}$, which define the width of the valley (low frequencies denote a wide valley, high frequencies a narrow valley).

(b) The coupling terms $\{B_{\mu,s}(s)\}$ and $\{B_{\mu,\nu}(s)\}$: They reflect the dynamic coupling between the motion along the path and the transverse vibrations as well as a coupling among the latter. Large $\{B_{\mu,s}(s)\}$ terms indicate that energy can flow non-adiabatically from translation to vibration and vice versa while the $\{B_{\mu,\nu}(s)\}$ terms determine the energy flow among the vibrations.[58]

From an analysis of the terms of the RPH, one obtains insight into qualitative features of reaction mechanism and reaction dynamics.

(1) By adding the change in the vibrational energy, $\Delta E^{\boldsymbol{n}}_{\text{vib}}(s)$ to the classical potential $V_0(s)$, one obtains the vibrationally adiabatic potential, which reflects the effect of vibrational energy on the reaction:

$$V^{\boldsymbol{n}}_{\text{vap}}(s) = V_0(s) + \Delta E^{\boldsymbol{n}}_{\text{vib}}(s) \tag{30}$$

where the $(3K-L)$-dimensional vector $\boldsymbol{n}$ denotes the vibrational state of the reaction complex, which according to the vibrationally adiabatic assumption does not change during the chemical reaction. In the harmonic approximation $\Delta E^{\boldsymbol{n}}_{\text{vib}}(s)$ is simply:

$$\Delta E^{\boldsymbol{n}}_{\text{vib}}(s) = \sum_{\mu}^{3K-L-1}\left(\boldsymbol{n}_\mu + \frac{1}{2}\right)\hbar[\omega_\mu(s) - \omega_\mu(-\infty)] = \sum_{\mu}^{3K-L-1}\left(\boldsymbol{n}_\mu + \frac{1}{2}\right)\hbar\Delta\omega_\mu(s) \tag{31}$$

For $\boldsymbol{n} = (0, 0, \ldots, 0)$, $V^0_{\text{vap}}(s)$ is the ground state adiabatic potential and $\Delta E^0_{\text{vib}}(s)$ is the *zero point energy* of the system at point s relative to that of the reactants ($s = -\infty$). If the frequency of one (or more) of the modes decreases substantially during the course of the reaction, e.g., as in a bond breaking process, then $\Delta\omega_\mu$ will be negative and vibrational excitation for that mode will lead to a reduction in the vibrationally adiabatic barrier for the reaction and a corresponding increase in the reaction rate.

(2) Energy dissipation during the course of the reaction involves energy transfer from one mode to the other. The magnitude of this transfer can be accessed by calculating the mode–mode coupling coefficients $B_{\mu,\nu}(s)$, which are given by the dot product between the normal mode vector $\boldsymbol{l}_\nu$ and the change of normal mode vector $\boldsymbol{l}_\mu$:[4,42]

$$B_{\mu,\nu}(s) = \{\boldsymbol{l}_\nu(s)\}^+\frac{d\boldsymbol{l}_\mu(s)}{ds} = -B_{\nu,\mu}(s) \tag{32}$$

where $\{\boldsymbol{l}_\mu(s); \mu = 1, 3K-L-1\}$ are the generalized normal mode vectors at point s. The $B_{\mu,\nu}(s)$ coefficients describe the mixing between modes μ and ν induced by the motion of the reaction complex along the RP. As this motion involves a rotation of the vibrational modes about the RP, the $B_{\mu,\nu}(s)$ terms are referred to as Coriolis couplings. Their meaning will become clear if one assumes that they are all equal to zero, i.e., there is no coupling between the transverse vibrational modes. In this situation, the character of all frequencies $\omega_\mu(s)$ should be preserved during the reaction, which is unlikely to happen. For example, the stretching frequency of a breaking bond will smoothly decrease to zero, thus crossing with frequencies $\omega_\mu(s)$ of other modes, some of which may have the same symmetry. Hence, there will be strong couplings and nonzero values of $B_{\mu,\nu}(s)$ in the case of avoided crossings, indicating that in these regions of the RP energy can readily flow from mode μ to mode ν.

(3) Translational–vibrational energy transfer during the course of the reaction can be described with the help of the coupling terms $B_{\mu,s}(s)$, which are given as the dot product between the reaction path vector $\boldsymbol{t}(s)$ and the change of the normal mode vector $\boldsymbol{l}_\mu(s)$:[4,42]

$$B_{\mu,s}(s) = \{\boldsymbol{t}(s)\}^+\frac{d\boldsymbol{l}_\nu(s)}{ds} = -\{\boldsymbol{l}_\mu(s)\}^+\frac{d\boldsymbol{t}(s)}{ds} = -\{\boldsymbol{l}_\mu(s)\}^+\boldsymbol{k}(s) \tag{33}$$

$B_{\mu,s}(s)$ describes the dynamic coupling between the RP and vibrational mode $\boldsymbol{l}_\mu(s)$. It is a measure of the mixing between the motion along the RP and the vibrational motion in mode μ induced by the curvature of the RP in the $(3K-L)$-dimensional space. As $B_{\mu,s}(s)$ becomes larger, the mixing between the RP and vibrational mode μ increases and energy transfer from translation to vibration and vice versa becomes more and more facile.[58] The total curvature of the RP is defined as:[4,42]

$$k(s) = \left[\sum_{\mu}^{3K-L-1} B_{\mu,s}^2(s)\right]^{1/2} = \{\boldsymbol{k}(s)^{+}\boldsymbol{k}(s)\}^{1/2} \qquad (34)$$

where $\boldsymbol{k}(s)$ is the curvature vector from equation (20)(see Figure 3).

(4) For a normal chemical reaction, the dynamic coupling between the motion along s and the motion along the $\{Q_\mu\}$ caused by the curvature of the RP must be explicitly taken into account. Translational to vibrational energy transfer during the course of a reaction occurs in regions where curvature $k(s)$ is large. In the entrance channel, modes which have large $B_{\mu,s}(s)$ values are donating modes, which means that vibrational excitation of these modes will cause energy to flow into the RP thus enhancing the rate of reaction. In the exit channel, modes with large $B_{\mu,s}(s)$ values are accepting modes. The reaction exoergicity can flow from the RP into these modes and lead to vibrational excitation of the products.

The curvature terms are intimately related to the well known propensity rules for abstraction reactions, in particular the rules put forward in the late 1960s by Polanyi and coworkers.[59] These authors found that for saddlepoints located in the exit channel, vibrational energy is far more effective than translational energy in overcoming the barrier to reaction. In this case, the curvature is expected to be large before the saddlepoint is reached. Translational energy will efficiently be drained into the transverse vibrational modes and, thus, no longer available for surmounting the barrier. On the other hand, vibrational energy in the modes strongly coupled to the RP will be transformed into translational motion along the RP and hence provides the energy needed to overcome the barrier. When large curvatures are found on the product side, just the opposite is true. Translational energy can be directly used to overcome the barrier while vibrational energy will be ineffective. The details, of course, depend on the magnitudes and variations of the curvature coupling terms, $B_{\mu,s}(s)$.

Within the framework of variational TS theory, it has been shown that the curvature of the RP, and hence the coupling terms, strongly influence quantum mechanical tunneling through the barrier.[60] The larger the coupling terms, the more facile tunneling is.

2.5 Calculation of the Terms of the Reaction Path Hamiltonian

The mass-weighted projected force constant matrix $\mathbf{K}(s)$ given by equation (25) has to be calculated and the eigenvalue problem (26) has to be solved to obtain for a given path point s $(3K-L-1)$ mass-weighted generalized normal modes and their associated frequencies. There are several strategies either to calculate generalized normal modes at each path point or at a selected number of path points. In any case, the number of evaluations has to guarantee smooth curves of generalized normal mode vectors $\boldsymbol{l}_\mu(s)$ and frequencies $\omega_\mu(s)$.

Since the calculation of the coupling coefficients requires the correlation of the vibrational modes along the RP, a prerequisite of using the RPH concept is that correct functions $\omega_\mu(s)$ are determined. To calculate the vibrationally adiabatic potentials, the vibrational energy levels of reactants, products, and TS must be properly ordered and correlated. Since an adiabatic RPH is used, functions $\omega_\mu(s)$ belonging to modes of the same symmetry obey the noncrossing rule, i.e., they must not cross.

Since most of the reactions investigated so far with the RPH possess symmetry, ordering has been done utilizing the symmetry of each vibrational function ('adiabatic ordering'). However, this ordering becomes problematic in the case of reactions without any symmetry and, therefore, diabatic ordering has been suggested,[61] which is based on the overlap between normal mode vectors calculated at two neighboring points s_m and s_{m+1} along the RP. Large overlap (>0.99) between two mode vectors at the two path points suggests that the corresponding normal mode frequencies represent points on the same function $\omega_\mu(s)$. Special care will have to be taken to determine the overlap in crossing and noncrossing regions, in particular if degenerate modes are involved. If two modes of the same symmetry interact only weakly, the corresponding functions $\omega_\mu(s)$ and $\omega_\nu(s)$ will approach each other rather closely before they depart. A resolution of the avoided crossing is obtained by automatically reducing the step size in the avoided crossing region and increasing it again after this path region.[61]

Once the functions $\omega_\mu(s)$ have been determined the coupling coefficients can be calculated. The Coriolis coupling coefficients involve the first derivative of the normal modes with regard to the reaction coordinate. For most *ab initio* methods, they cannot be calculated analytically since they involve third derivatives of the energy. Accordingly, they are calculated by finite difference techniques where one exploits the fact that the matrix of $B_{\mu,\nu}$ coefficients is antisymmetric $(B_{\mu,\nu} = -B_{\nu,\mu})$ for any point s and that coefficients involving modes of different symmetry vanish. The curvature coupling coefficients are calculated by finite difference techniques multiplying the first derivative of a given normal mode with the reaction path vector. Alternatively, they can be calculated analytically as the product of normal mode vector and curvature vector where calculation of the latter requires just gradient and Hessian matrix (see equations 33 and 20). Since the reaction path vector is totally symmetric, curvature couplings involving normal modes of lower symmetry also vanish. Once the curvature coupling coefficients are calculated, the curvature of the RP is calculated with the help of equation (34).

2.6 Methods for Analyzing Elements of the Reaction Path Hamiltonian

Chemists usually understand the geometry and conformation of a molecular system such as the reaction complex in terms of internal coordinates. Therefore, it is logical to decompose the reaction path vector in terms of internal coordinates and to see which coordinate is dominating the direction of the path. For the same reason, it is useful to express the energy gradient in terms of internal coordinates so that the forces exerted on the nuclei at a given path point can be analyzed in connection with the geometrical description of the reaction complex.

It is more difficult to understand changes in normal modes and coupling coefficients along the RP in terms of simple geometrical pictures based on internal coordinates. Normal modes $\boldsymbol{l}_\mu$ are delocalized modes that in most cases cannot be correlated with localized or internal modes, each of which is associated with just one particular internal coordinate. The ideal case for a chemist to interpret vibrational motions would be that for each normal mode the relationship $\boldsymbol{l}_\mu = \boldsymbol{v}_n$ holds where $\boldsymbol{v}_n$ is a localized internal mode such as, for example, the stretching mode of a bond (associated with the bond length), the bending motion of a three-atom unit (associated with the bond angle), or a twisting mode of a four-atom unit (associated with a torsional angle). However, because of electronic and mass coupling internal vibrational modes mix to yield delocalized normal modes, which can no longer be associated with a single internal coordinate.

2.6.1 *Analysis of Normal Modes and Curvature Vector*

Konkoli and Cremer[62] have recently suggested internal vibrational modes that are suited to analyzing delocalized normal modes in terms of local modes. Their definition of internal modes is based on the fact that mass coupling between internal modes is much stronger than electronic coupling. If one can suppress mass coupling, then a solution for the definition of a local mode associated with just one internal coordinate can be found. Konkoli and Cremer solved the problem by modifying the Euler–Lagrange equations in such a way that all nuclear masses (and thus also all momenta) of a molecule, except those of the nuclei associated with a particular internal coordinate, are set to zero. In this way, the modified Euler–Lagrange equations define a set of local modes that are strictly constrained to that molecular fragment, which is described by the internal coordinate in question.

The internal modes thus obtained are called adiabatic modes because they can alternatively be viewed as those modes that result when minimizing the energy of a vibrating molecule by relaxing for a given vibrational mode all nuclear positions except those defined by the pulsation of the internal coordinate in question.[61] Adiabatic internal vibrational modes comply with the symmetry of the molecule and are independent of the choice of the set of internal coordinates used to describe the molecule. Furthermore, they are perfectly suited to characterize normal vibrational modes in the common language of chemistry that attempts to express molecular properties in the form of internal coordinates.

Adiabatic internal modes can be defined for equilibrium points on the PES as well as for all points along the RP where in the latter case it is required that the harmonic part of the energy in equation (28b) is minimized with regard to displacements in the $(3K - L - 1)$-dimensional vibrational space while relaxing all internal parameters but one. In this way, generalized adiabatic modes $\boldsymbol{a}_k(s)$ together with the corresponding adiabatic frequencies $\omega_k(s)$ and force constants $k_k(s)$ are calculated where k denotes a particular internal coordinate R_k.

With the help of the generalized adiabatic modes $\boldsymbol{a}_k(s)$, both normal modes $\boldsymbol{l}_\mu(s)$ and curvature vector $\boldsymbol{k}(s)$ can be analysed utilizing appropriately defined amplitudes $A_{k,\mu}(\boldsymbol{l}; s)$ and $A_{k,s}(\boldsymbol{k}; s)$:[63]

$$A_{k,u}(\boldsymbol{l}, s) = \frac{[\boldsymbol{l}_\mu^+(s)\mathbf{F}(s)\boldsymbol{a}_k(s)]^2}{[\boldsymbol{a}_k^+(s)\mathbf{F}(s)\boldsymbol{a}_k(s)][\boldsymbol{l}_\mu^+(s)\mathbf{F}(s)\boldsymbol{l}_\mu(s)]} \tag{35}$$

$$A_{k,s}(\boldsymbol{k}, s) = \frac{[\boldsymbol{k}^+(s)\mathbf{M}(s)\boldsymbol{a}_k(s)]}{[\boldsymbol{a}_k^+(s)\mathbf{M}(s)\boldsymbol{a}_k(s)]^{1/2}} \tag{36}$$

which describe generalized normal modes (equation 35) and the curvature vector $\boldsymbol{k}(s)$ (equation 36) in terms of generalized adiabatic modes associated with internal coordinates used in the description of the reaction complex. The matrix $\mathbf{F}$ guarantees a dynamic characterization of normal modes while the matrix $\mathbf{M}$ provides a kinetic characterization. Amplitude $A_{k,s}$ has the same dimension as $B_{\mu,s}$ and, for $\boldsymbol{l}_\mu = \boldsymbol{a}k$, amplitude $A_{k,s}$ and coefficient $B_{\mu,s}$ are equal.

2.6.2 *Analysis of the Reaction Path Vector*

Kato and Morokuma[58] suggested a procedure for analyzing the reaction path vector in terms of basis vectors $\boldsymbol{u}^k(s)$:

$$\boldsymbol{u}_k(s) = \mathbf{M}^{-1}(s)\boldsymbol{b}_k(s) \tag{37}$$

where $\boldsymbol{b}_k$ is a vector of the $\mathbf{B}$ matrix, see equation (15).

Konkoli, Kraka, and Cremer[63] have shown that the basis vectors $\boldsymbol{u}_k$ correspond to the internal modes that characterize the movement along the RP and, therefore, represent the equivalent to the adiabatic internal modes which are used for the analysis of the transverse normal vibrational modes. Accordingly, an amplitude $A_{k,s}$ based on the matrix $\mathbf{M}$ can be defined as:

$$A_{k,s}(\boldsymbol{t}, s) = \frac{[\boldsymbol{g}^+(s)\mathbf{M}^{-1}(s)\boldsymbol{b}_k(s)]^2}{[\boldsymbol{g}^+(s)\mathbf{M}^{-1}(s)\boldsymbol{g}(s)][\boldsymbol{b}_k^+(s)\mathbf{M}^{-1}(s)\boldsymbol{b}_k(s)]} \tag{38}$$

which considers the kinetic aspect of the translational motion along the RP. With these amplitudes, the reaction path vector can be decomposed into internal coordinate components for each point along the RP.

2.6.3 *Calculation of Other Properties Along the Reaction Path*

Once all elements of the RPH have been determined, the evolution of the reaction complex along the RP can be displayed. For example, plots of the internal coordinates in dependence of s provide valuable information about the way the reacting atoms approach each other, interact, and then separate. In the case of polyatomic systems these two-dimensional pictures display the complex structural changes taking place in $(3K - L)$-dimensional space in an understandable form and can be used to generate three-dimensional images of the structural changes along the RP.

When calculating the elements of the RPH, it does not require much additional effort to calculate also other properties of the reaction complex that depend on s. An example can be found in the investigation of the isomerization reaction of the methoxy radical to the hydroxymethyl radical by Colwell and Handy,[64] where the authors also determined the dipole moment and the components of the polarization tensor as a function of s. A systematic step in this reaction has been made by Konkoli, Kraka, and Cremer,[63] who analyzed the *electron density* distribution $\rho(\boldsymbol{r}, s)$ of the reaction complex along the RP, calculating difference density distribution $\Delta\rho(\boldsymbol{r}, s)$ (equation 39), Laplace concentrations $\nabla^2\rho(\boldsymbol{r}, s)$,

and difference Laplace concentrations (equation 40):

$$\Delta\rho(\boldsymbol{r}, s) = \rho(\boldsymbol{r}, s)[\text{reaction complex}] - \rho(\boldsymbol{r}, s)[\text{procomplex}] \quad (39)$$

$$\Delta\{\nabla^2\rho(\boldsymbol{r}, s)\} = \nabla^2\rho(\boldsymbol{r}, s)[\text{reaction complex}] - \nabla^2\rho(\boldsymbol{r}, s)[\text{procomplex}] \quad (40)$$

as well as response properties such as multipole moments and other one-electron properties. If difference density distributions are used, particular care has to be taken with regard to the choice of the reference density of the procomplex and the correction of basis set superposition errors.

Plots of the molecular orbitals or the electron density along the RP provide valuable insight into electronic effects which govern the reaction and can be discussed in connection with the energetics of the reaction, structural changes, changes in forces, force constants, coupling coefficients, etc., thus providing a very detailed description of the reaction. In Table 2, a summary of RP, reaction valley, and reaction complex properties and their impact on reaction mechanism and dynamics of chemical reactions is given.

Table 2 Reaction Path, Reaction Valley, and Reaction Complex Properties

Property		Information
1. Reaction Path		
IRC	s	Length of RP
Classical potential	$V_0(s)$	Height of RP
Reaction path vector	$\boldsymbol{t}(s)$	Direction of RP
Coordinate amplitude	$A_{ks}(\boldsymbol{t}; s)$	Dominant internal coordinate of $\boldsymbol{t}(s)$
Curvature vector	$\boldsymbol{k}(s)$	Curvature of RP
Rotation of $\boldsymbol{k}(s)$-plane	$\tau(s)$	Distinction of reaction phases
2. Reaction Valley		
Normal mode coordinates	$Q_\mu(s)$	Direction of the valley
Normal mode frequencies	$\omega_\mu(s)$	Curvature of the valley
Adiabatic force constants and frequencies	$k_a(s)$ $\omega_a(s)$	Curvature of the valley in internal coordinates
Adiabatic amplitudes	$A_{k\mu}(\boldsymbol{l}; s)$	Analysis of normal modes
Curvature couplings	$B_{\mu s}(s)$	Energy transfer and rate enhancement
Adiabatic mode-curvature couplings	$A_{ks}(\boldsymbol{k}; s)$	Influence of adiabatic modes on curvature
Coriolis couplings	$B_{\mu\nu}(s)$	Energy dissipation
3. Reaction Complex		
Classical potential	$V_0(s)$	Energetics of reaction
Internal coordinates	$\boldsymbol{R}(s)$	Geometry of complex
Moments of inertia tensor	$\mathbf{I}_s(s)$	Rotation of complex
Internal forces	$f_k(s)$	Attraction, repulsion between atoms
Electron density	$\rho(\boldsymbol{r}; s)$	Electronic structure of reaction complex
Laplace concentration	$-\nabla^2\rho(\boldsymbol{r}; s)$	
Atomic charges	$q_K(s)$	
Dipole moment	$\mu(s)$	
Polarizability	$\alpha(s)$	
Magnetic susceptibility	$\chi(s)$	

Information on reaction dynamics: $V_0(s)$, $\mathbf{I}_s(s)$, $\omega_\mu(s)$, $B_{\mu s}(s)$, $B_{\mu\nu}(s) \rightarrow$ rate constant, tunneling effect, prediction of vibrational mode specific enhancement of reaction rates, vibrational energy dissipation, product vibrational state distributions

Information on reaction mechanism: $V_0(s)$, $\boldsymbol{R}(s)$, $f_k(s)$, $\rho(\boldsymbol{r}; s)$, $-\nabla^2\rho(\boldsymbol{r}; s)$, $q_K(s)$, $\mu(s)$, $\alpha(s)$, $\chi(s)$, $\boldsymbol{t}(s)$, $A_{ks}(\boldsymbol{t}; s)$, $\boldsymbol{k}(s)$, $A_{ks}(\boldsymbol{k}; s) \rightarrow$ distinction of reaction phases, location of van der Waals region and TS region, sequencing of bond breaking and bond forming processes, analysis in terms of attractive and repulsive forces, dependence on substituents

2.7 Modifications and Extensions of the RPH

Since the RPH concept is based on several assumptions, relaxation of one or more of these assumptions leads to more general RPH approaches. Also, there are chemical reactions for which the original RPH of Miller, Handy, and Adams[4] can no longer be applied because of its limitations and then extensions of the concept become necessary. Figure 5 is an overview of the modifications and extensions of the original RPH concept which will be discussed in the following text.

2.7.1 *The Diabatic Reaction Path Hamiltonian*

Although in many cases a reasonable simplification, it is certainly more realistic to abandon the assumption of a harmonic reaction valley and to use a valley potential with appropriate anharmonic corrections. Hence, the potential energy part in the RPH adopts the form of equation (41):[7,65]

$$V(s, \{Q_u\}) = V_0(s) + \frac{1}{2!}\sum_\mu \omega_\mu^2(s)Q_\mu^2(s) + \frac{1}{3!}\sum_\mu\sum_\nu\sum_\lambda C_{\mu\nu\lambda}(s) \times Q_\mu(s)Q_\nu(s)Q_\lambda(s) + \frac{1}{4!}\sum_\mu\sum_\nu\sum_\lambda\sum_\sigma C_{\mu\nu\lambda\sigma}(s) \times Q_\mu(s)Q_\nu(s)Q_\lambda(s)Q_\sigma(s) \quad (41)$$

where the coefficients of the cubic and the quartic term are given by:

$$C_{\mu\nu\lambda}(s) = \sum_i\sum_j\sum_k \frac{\partial^3 V(s)}{\partial x_i \partial x_j \partial x_k} l_{i,\mu}(s) l_{j,\nu}(s) l_{k,\lambda}(s) \quad (42)$$

and

$$C_{\mu\nu\lambda\sigma}(s) = \sum_i\sum_j\sum_k\sum_l \frac{\partial^4 V(s)}{\partial x_i \partial x_j \partial x_k \partial x_l} l_{i,\mu}(s) \times l_{j,\nu}(s) l_{k,\lambda}(s) l_{l,\sigma}(s) \quad (43)$$

The coefficients C cover (besides intramode anharmonic contributions) mode–mode coupling in the potential energy part of the RPH and, therefore, are called potential energy couplings. Contrary to the original adiabatic RPH, frequencies $w_\mu(s)$ corresponding to modes of the same symmetry can now cross, i.e., they undergo a local Fermi resonance in the crossing region. A RPH corresponding to the potential of equation (41) is called a diabatic RPH.

A diabatic RPH may also be used within the harmonic reaction valley approach when one considers not the curved RP but a least motion path that interpolates linearly between two boundary points of a path region with strong curvature (see Section 2.7.4). Such a 'straight line' path is useful for tunneling descriptions in connection with hydrogen transfer reactions.[66] The kinetic part of the RPH no longer contains curvature couplings since a straight line has zero curvature. The remaining Coriolis couplings in the kinetic energy can be

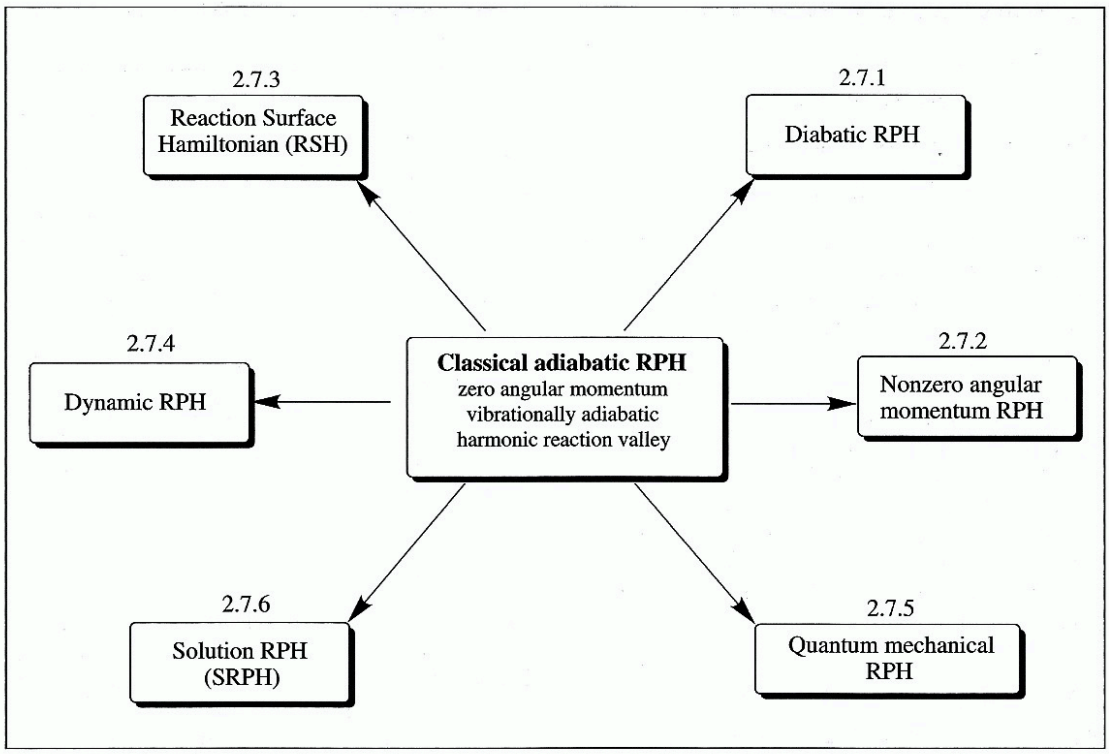

Figure 5 Overview of modifications and extensions of the RPH concept (numbers refer to the section in which a particular extension of the RPH is discussed)

transferred to the potential energy part by an appropriate transformation so that the kinetic energy part no longer contains coupling terms, which is important if one wants to quantize the RPH. The potential V along the straight line path adopts the form of equation (44):[66]

$$V(s, \{Q_\mu\}) = V_0(s) - \sum_\mu C_\mu(s) Q_\mu(s) + \frac{1}{2} \sum_\mu \sum_\nu Q_\mu(s) \Lambda_{\mu,\nu}(s) Q_\nu(s) \qquad (44)$$

where the linear term is a direct consequence of the fact that the straight line path is no longer a minimum energy path. The diagonal elements $\Lambda_{\mu,\mu}(s)$ can be interpreted as diabatic frequencies, which can cross independent of the symmetry of the corresponding normal modes. The off-diagonal elements $\Lambda_{\mu,\nu}(s)$ in the potential coupling terms describe transitions from mode μ to mode ν. Despite the harmonic approximation of the potential given in equation (44) the associated RPH is diabatic.[66]

2.7.2 *Inclusion of Total Angular Momentum*

A more realistic RPH approach should include angular momentum $\boldsymbol{J}$ by considering the rotational symmetry of a polyatomic reaction complex in three-dimensional space and the conservation of total angular momentum.[36] For this purpose, the three components of $\boldsymbol{J}$, J_x, J_y, and J_z, must be expressed in terms of the canonical variables of rotation, e.g., by using the action-angle variables (J, q_J), (M, q_M), (K, q_K), where J is the magnitude of $\boldsymbol{J}$, M and K its projection onto space-fixed and body-fixed z-axes, and q_J, q_M, q_K their conjugated angle variables.[67] Since J and M are conserved quantities, the Hamiltonian does not depend on q_J and q_M. The direction of the space-fixed axis is arbitrary and, therefore, the Hamiltonian is also independent of M. For a given value of $\boldsymbol{J}$, the rotational part of the Hamiltonian can be written as:[67]

$$\varepsilon_{\text{rot}}^J(K, q_k; s) = A(s)(J^2 - K^2)\cos^2 q_K + B(s)(J^2 - K^2)\sin^2 q_K + C(s)K^2 \qquad (45)$$

where $A(s)$, $B(s)$, $C(s)$ are the rotational constants for a given value of s.

New types of coupling terms have to be considered, which describe the coupling between rotation and the motion along the path and the coupling between rotations and vibrations.[4] The latter is described (in first order) by the cross-product of the eigenvectors of the transverse vibrational modes and by centrifugal distortion terms.[4]

2.7.3 *From a Reaction Path to a Reaction Surface*

In the case of the reaction $\text{Cl} + \text{HCl} \rightarrow \text{ClH} + \text{Cl}$, which in view of the masses of the atoms involved can be called a 'heavy–light–heavy' atom transfer reaction, the RP is sharply curved.[68] As a consequence, the dynamic motion of the reaction complex deviates strongly from the RP into the region of strong curvature. Similar observations can be made in other hydrogen transfer reactions. In these cases, the basic assumption of the original RPH, namely that the $(3K - L)$-dimensional coordinate space can be spanned by one LAM being connected with the displacements s along the RP and $(3K - L - 1)$ small amplitude motions (SAM) being associated with the normal coordinates Q_μ orthogonal to the RP,

breaks down. One has to treat all LAMs (the 'system') separately from the SAMs (the 'bath') in the RPH to obtain a reasonable description of the dynamics of the reaction.[69]

Nauts and Chapuisat[7] proposed partitioning the $(3K - L)$ internal coordinates of the reaction complex into n internal coordinates R_k^S, which provide a description of the LAMs, and $(3K - L - n)$ normal coordinates Q_μ describing the SAMs. The coordinates R_k^S span an n-dimensional reaction surface (reaction hypersurface, reaction volume, reaction hypervolume), which is orthogonal to the remaining $(3K - L - n)$-dimensional subspace of the SAMs. For a minimum energy surface, zero angular momentum, and harmonic energy walls, the reaction surface Hamiltonian (RSH) takes the form of equation (46):[8]

$$H[\{R_k^s\}, \{P_k\}, \{Q_\mu\}, \{P_\mu\}] = \frac{1}{2}(P_R^+, P_Q^+)\begin{pmatrix} G_{RR} & G_{RQ} \\ G_{QR} & G_{QQ} \end{pmatrix}\begin{pmatrix} P_R \\ P_Q \end{pmatrix} + V_0(\boldsymbol{R}^s) + \frac{1}{2}\sum_\mu \omega_\mu^2(\boldsymbol{R}^s)Q_\mu^2(\boldsymbol{R}^s) \quad (46)$$

where the matrix $\mathbf{G}$ (related to the Wilson $\mathbf{G}$ matrix) is partitioned into elements G_{RR}, G_{QQ}, etc., according to a partitioning of the total space into the space of the surface coordinates $\{R_k^S\}$ and the space of the normal mode coordinates $\{Q_\mu\}$. Couplings between on- and off-surface modes are covered by the elements of the $\mathbf{G}_{QR}$ submatrix.

There are several obstacles that make the use of the RSH difficult. First, the choice of the coordinates $\{R_k^S\}$ is not trivial and requires either chemical intuition or a preliminary calculation with the RPH that reveals all LAMs. Once coordinates R_k^S have been selected, the reaction surface has to be mapped out by constrained geometry optimizations for a grid of $\{\boldsymbol{R}^S\}$ points. This in itself can be already very time consuming apart from the fact that an analytical function $V_0(\boldsymbol{R}^S)$ has to be derived to carry out the dynamics calculations. Frequencies, normal modes, and coupling coefficients are complicated functions of $\boldsymbol{R}^S$, which are difficult to calculate and to interpret.

If coordinates $\boldsymbol{R}_k^S$ are correctly determined and the reaction surface embodies all LAMs determining the dynamics of the reaction, then the coupling with the transverse vibrational modes will be small. It is possible to neglect all off-diagonal $\mathbf{G}$-matrix elements, which contain these couplings, and to use a zeroth-order RSH, which is still practical. In this way, the RSH has been used to investigate the intramolecular proton transfer in malonaldehyde[70] or the double proton transfer in the formic acid dimer.[71] It has been shown that tunneling is reasonably described when using the RSH; however, depending on the choice of the reaction surface coordinates, tunneling splittings can differ by several orders of magnitude.[9]

2.7.4 *The Dynamic Reaction Path Hamiltonian*

Recently, Taketsugu and Gordon[72] suggested a 'dynamic' RPH based on reaction coordinate s and a curvature coordinate ρ that should be effective when the RP is sharply curved and the original adiabatic RPH becomes inappropriate. The dynamic RPH generalizes the natural collision coordinates of Marcus (used to describe a collinear reaction of the type $A + BC \rightarrow AB + C$[53]) to a K-atomic reaction complex. The curvature coordinate ρ defines displacements along the curvature vector $\boldsymbol{k}(s)$ and, accordingly, is suited to describe any coupling between the translational motion along the RP and a transverse vibrational motion that causes a large curvature vector. Couplings with the remaining $(3K - L - 2)$ normal modes $\boldsymbol{l}_\mu$ do not play any role and can be ignored. Hence, the RPH takes in this case the form of equation (47):[72]

$$H[s, p_s, \rho, p_\rho, \{Q_\mu\}, \{P_\mu\}] = \frac{1}{2}\frac{p_s^2}{[1 + \rho k(s)]^2} + V(s) + \frac{1}{2}p_\rho^2 + \frac{1}{2}\omega_\rho^2(s)\rho^2 + \sum\left[\frac{1}{2}P_\mu^2 + \frac{1}{2}\omega_\mu^2(s) \times Q_\mu^2(s) - k_{\mu,\rho}(s)Q_\mu(s)\right] \quad (47)$$

where p_ρ is the conjugated momentum of ρ, $k_{\mu,\rho}(s) = \partial V^2(s)/\partial Q_\mu \partial_\rho$ is an off-diagonal element of the force constant matrix, which describes a potential energy coupling between ρ and Q_μ. Coriolis coupling terms of the $(3K - L - 2)$ normal modes are neglected. Kinetic energy coupling between s and ρ is described by the term $\rho k(s)$ while couplings between s and Q_μ are covered by the curvature $k(s)$.

The dynamic RPH is related to the RSH (Section 2.7.3) in so far as a reaction surface is used in the form of a flexible reaction plane defined by the reaction path vector $\boldsymbol{t}(s)$ and the curvature vector $\boldsymbol{k}(s)$ (see Figure 6). Since the curvature vector orients itself at each new path point in configuration space the reaction plane always adjusts to the direction of strongest RP curvature. Accordingly, use of the reaction plane does not require a preselection of LAM coordinates and the calculation of a minimum energy reaction surface. In addition, the rotation of the reaction plane provides a measure for determining the sequence of interactions between translational motion and transverse LAMs.[72] All LAMs and all deviations from the RP because of sharp curvature are covered without increasing the dimensions of the reaction surface. Of course, in those

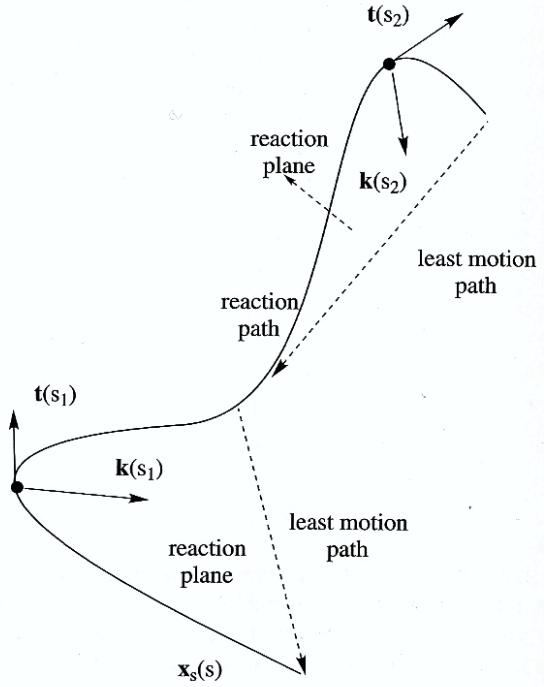

Figure 6 Schematic illustration of a RP with two reaction planes defined by reaction path vector and curvature vector at path positions s_1 and s_2

regions where there are rapid changes in the reaction plane, the reacting system will move away from the two-dimensional plane and then the more complete description by the RSH is appropriate.

2.7.5 *A Quantum Mechanical RPH*

Only a few attempts have been made to replace the classical RPH by a (semi-)quantum mechanical RPH. For example, this can be done for the kinetic part of the RPH by replacing all momenta by the corresponding quantum mechanical operators. This is particularly easy in the case of a diabatic RPH based on a zero curvature ('straight line') RP assumption for which all coupling terms are removed from the kinetic energy.[4] Also, the harmonic potential can be quantized, as done by Billing,[73] who derived in this way a semi-classical RPH that is useful for dynamics calculations (see ***Mixed Quantum–Classical Methods***).

2.7.6 *A Solution Reaction Path Hamiltonian (SRPH) for Reactions in Polar Solvents*

The RPH concept has been used by Lee and Hynes[10] to develop a model for the description of chemical reactions in polar solvents where the solvent is treated as a polarizable continuum characterized by its dielectric constant. The progress of the reaction from reactants to products is described by a single coordinate X_{Re} (ignoring any other internal molecular modes), which is chosen on the basis of chemical intuition rather than rigorous definition. For example, in the case of the ionic dissociation $AB \rightarrow A^+ + B^-$ the reaction coordinate X_{Re} is simply the distance between atoms A and B.

Essential for the approach of Lee and Hynes[10] is the variation of the charge distribution in the reaction complex with X_{Re}. In the ionic dissociation reaction, the charge on each atom will increase strongly along the RP and, as a consequence, solvation will become stronger with increasing X_{Re}. This increase in charge is described by charge distribution functions for each atom of the reaction complex that cover the limiting cases of reactant and product. Solvent polarization, and thus the free enthalpy $G_{eq}(X_{Re})$ of the reaction complex in the solvent, is calculated for each point along the RP using the charge distribution functions. Any deviation from the solvent polarization obtained for a path point X_{Re} is measured by a solvent coordinate X_{Sol}, which is defined by a different charge distribution in the reaction complex at X_{Re} and the corresponding nonequilibrium solvent polarization. By analogy with the RPH, the coordinate X_{Re} is associated with the LAM along the RP while coordinate X_{Sol} corresponds to an orthogonal motion covering all solvent rearrangements. A harmonic reaction valley is described by the free enthalpy function $G(X_{Re}, X_{Sol})$:

$$G(X_{Re}, X_{Sol}) = G_{eq}(X_{Re}) + \tfrac{1}{2}K_{Sol}(X_{Re})[\Delta X_{Sol}(X_{Re})]^2 \quad (48)$$

where the first term is the equilibrium free enthalpy, i.e., the solvent polarization has adjusted to the charge distribution of the reaction complex at point X_{Re}, and the second term gives the free enthalpy part due to deviation from equilibrium polarization at X_{Re}.

As indicated in Figure 7 any displacement ΔX_{Sol} leads to an increase of the free enthalpy, and thus a valley emerges that can be described by the harmonic approximation of equation (48).

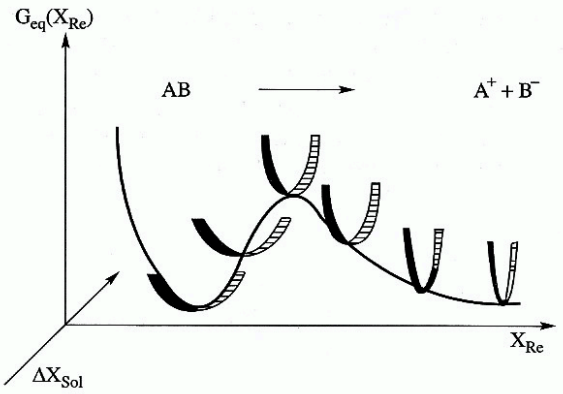

Figure 7 Schematic illustration of the free enthalpy reaction valley for the ionic dissociation $AB \rightarrow A^+ + B^-$ in a polar solvent. The solvent becomes more stiff as X_{Re} increases

Lee and Hynes[10] show that the steepness of the solvation valley can be described by a 'force constant' $K_{Sol}(X_{Re})$, which is related to the solvent polarization mass $\mu_{Sol}(X_{Re})$ and a solvent frequency ω_{Sol}, which is independent of the reaction coordinate:

$$\mu_{Sol}(X_{Re}) = \omega_{Sol}^{-2}K_{Sol}(X_{Re}) \quad (49)$$

Figure 7 shows that with increasing charge on atoms A and B (increasing X_{Re}) of an ionic dissociation reaction a deviation from the equilibrium polarization of the solvent becomes more and more difficult because of the increasing steepness of the solvent valley. In other words, solvation plays a larger role for the generated ions than for the neutral AB molecule.

Despite the simplified choice of the coordinate system, it is possible to define intrinsic reaction coordinates, which becomes somewhat more difficult than for the gas phase RPH because of the dependence of the effective solvent polarization mass on the coordinate X_{Re}.[10] In terms of the intrinsic coordinates x_{Re} and x_{Sol}, the SRPH is given by:

$$H(x_{Re}, p_{Re}, x_{Sol}, p_{Sol}) = \frac{1}{2\Delta(x)}(p_{Re}^2 + p_{Sol}^2) + G(x_{Re}, x_{Sol}) \quad (50)$$

where $\Delta(x)$ is a scale factor defined by the effective solvent polarization mass at the TS. Evaluating the IRC path as a sequence of points, with s being the arc length along the path, the changes of the reaction complex in solution can be discussed as functions of s as in the case of the original RPH model. By combining the SRPH model with variational TS theory, reaction rates of reactions in polar solvents can be evaluated.[10]

3 APPLICATIONS

Since 1980, a considerable number of investigations has been carried out which utilized the RPH of Miller, Handy, and Adams[4] or one of its extensions. Most of these calculations focused on reaction dynamics and presented rate constants, tunneling effects, or other dynamic properties of chemical reactions. Since these topics are covered by other articles of this volume, in this article a summary of the mechanistic information obtained from an application of the RPH is discussed.

3.1 An Overview of Applications Based on the RPH

Table 3 gives some information on those RPH studies carried out since 1980, which provide in addition to reaction dynamics some insight into the reaction mechanism, e.g., by showing and discussing the dependence of energy, geometry, frequencies, and coupling coefficients on the reaction coordinate s. There are a number of points that become obvious when considering the work summarized in Table 3.

(1) Most reaction systems investigated so far with the help of the RPH or its extensions are rather simple, comprising just two- or three-heavy-atom systems.
(2) The majority of *ab initio* methods employed in these studies are of the low level type and provide little accuracy.
(3) Apart from cost considerations that dictate the choice of the *ab initio* method used, there are still technical difficulties in calculating the elements of the RPH.
(4) In most of the RPH studies published so far, the mechanistic information provided by this approach is not fully exploited.

However, there is recent work indicating that some or all of these shortcomings will be overcome in the near future. For example, Konkoli, Kraka, and Cremer[61] have improved the RPH approach so that it can readily be applied to reaction systems with six and more heavy atoms as their investigation of the Diels–Alder reaction between ethene and butadiene shows. There are some applications that use modern correlation corrected methods such as MP2, QCISD, or GVB-CISD (Table 3). Particularly promising seems to be the use of DFT although further improvements of DFT are needed[88] to describe loosely bound TSs and the reaction complex in the van der Waals region of the RP. DFT is attractive because of its relatively low computational cost and the fact that a considerable part of correlation corrections is covered, which gives DFT results of MP2 or even better accuracy.

There is also a large potential in dual level methods[11] that provide a systematic basis for scaling potential function, frequency functions, and other s-dependent properties obtained at lower levels of theory with the help of high-accuracy calculations at selected points along the RP. More experience is needed to make scaling a reliable procedure and to obtain in

Table 3 Applications of the RPH and its Extensions with Emphasis on *Ab Initio* Based RP Studies

	Reaction	Method	Basis set	Authors	Year	Ref.
I. RPH studies						
1	$HCN \rightarrow CNH$	HF	DZP	Gray, Miller	1980	74
2	$H_2CO \rightarrow H_2 + CO$	HF	DZ	Waite, Gray, Miller	1983	75
3	$H_2C{=}C: \rightarrow H\text{-}C{\equiv}C\text{-}H$	CIDS	TZ + P	Carrington, Miller,	1984	8
4	$CH_3O \rightarrow CH_2OH$	ROHF	DZ	Colwell, Handy	1985	64
5	$Li + FH \rightarrow LiF + H$	CISD	DZ + P + diff	Dunning, Kraka, Eades	1987	76
6	$OH + H_2 \rightarrow H_2O + H$	GVB-CISD	VDZ + P	Dunning, Harding, Kraka	1989	77
7	$H + HCO \rightarrow H_2 + CO$	MCSCF	VDZ + P	Dunning, Harding, Kraka	1989	77
8	$CH_3 + H_2 \rightarrow CH_4 + H$	UHF	STO-3G	Baldrige et al.	1989	78
9	$CH_3 + H_2 \rightarrow CH_4 + H$	UQCISD	6-311G(d,p)	Truong	1994	81
10	$CH_3 + H_2 \rightarrow CH_4 + H$	DFT	6-311G(d,p)	Truong, Duncan	1994	82
11	$CH_3 + H_2 \rightarrow CH_4 + H$	UMP2	6-31G(d,p)	Konkoli, Kraka, Cremer	1996	63
12	$H^- + CH_3F \rightarrow CH_4 + F^-$	HF	4-31G	Ryaboy	1989	79
13	aziridine inversion[a]	HF	3-21G	Rom, Ryaboy, Moiseyev	1993	80
14	$CH(^4\Sigma^-) + H_2 \rightarrow CH_2(^3B_1) + H$	UHF	6-31G	Liu, Ma, Li	1994	83
15	$H + H\text{-}CC\text{-}H \rightarrow H\text{-}CC + H_2$	UHF	6-31G	Fang, Fu	1994	84
16	$CH_4 + Pd \rightarrow CH_3\text{-}Pd\text{-}H$	CNDO/S		Mamaev et al.	1995	85
17	$CH_4 + F \rightarrow CH_3 + FH$	UMP2	6-31G(d,p)	Corchado, Espinosa-Garcia	1996	86
18	$C_2H_4 + FH \rightarrow CH_3CFH_2$	HF	4-31G	Kato, Morokuma	1980	58
19	$C_2H_4 + FH \rightarrow CH_3CFH_2$	MP2	6-31G(d,p)	Kraka et al.	1997	87
20	$C_4H_6 + C_2H_4 \rightarrow C_6H_{10}^b$	HF	6-31G(d)	Kraka et al.	1997	87
II. Extended RPH studies						
21	H transfer in malonealdehyde[c]	RHF	STO-3G	Carrington, Miller	1986	70
22	H,H transfer in formic acid dimer	HF + MCPF	MIDI4	Shida, Barbara, Almlöf	1991	71
23	$OH + H_2 \rightarrow H_2O + H$	analytical PES		Billing	1990	73
24	$Cl^- + CH_3Cl \rightarrow ClCH_3 + Cl$	analytical PES		Billin	1992	73
25	$Cl^- + CH_3Cl \rightarrow ClCH_3 + Cl^-$	analytical PES		Lee, Hynes	1988	10
26	$CH_3 + H_2 \rightarrow CH_4 + H$	CASSCF	6-31G(d,p)	Taketsugu, Gordon	1996	72
27	$H_2C{=}S$	MP2	6-31G(d,p)	Minichino, Barone	1994	65

a

b

c

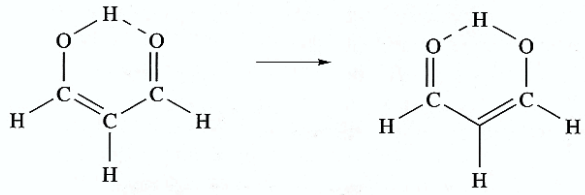

this way useful RPH descriptions at relatively low computational cost.

In general, the RP is investigated only in the immediate vicinity of the TS. This has to do with cost considerations and the fact that some RP following algorithms fail in the van der Waals region where the PES becomes rather flat and where it is difficult to find the floor-line of a more and more vanishing reaction valley. Oscillations in the tailing parts of the RP curvature or the coupling coefficients document these difficulties and are mostly the reason why the RP search is stopped at a rather early point, excluding most of the van der Waals region (see Section 3.2.2). Often there are also kinks or other inconsistencies in published graphs of $\omega_\mu(s)$, coefficients $B_{\mu\nu}(s)$ or $B_{\mu s}(s)$ even in the TS region, which clearly are a result of deficiencies of the algorithms used or the choice of an inappropriate step size Δs. A particular critical point is the ordering of frequencies $\omega_\mu(s)$ along the RP which, for example, is needed to get correct mode–mode and curvature coupling coefficients. Most of the reaction systems listed in Table 3 possess relatively high symmetry, which makes an adiabatic ordering of frequencies 'by hand' possible as becomes obvious from some of the published graphs. An automated diabatic ordering method has recently been worked out by Konkoli, Kraka, and Cremer, which can solve this problem and which has successfully been applied to reaction complexes with more than 40 vibrational frequencies.[61]

Yet another technical problem is the numerical differentiation, which is applied to calculate RP curvature and coupling coefficients. This problem is related to the choice of the step size Δs, which when chosen to be rather small leads to a rapid increase of calculational cost, but when chosen too large implies a contamination of calculated derivatives by higher-order derivatives. The consequences of the latter choice are, for example, false curvature peaks, inaccurate values of curvature and coupling coefficients, as well as a blurring of fine features of these quantities. A solution to this problem should be provided by the use of variable step sizes along the RP, namely large step sizes in those regions which are not interesting for mechanistic and dynamic investigations, and small step sizes in all other regions of the RP.

Apart from these technical and method related problems, characteristic of most of the RPH studies listed in Table 3, there is also a basic problem. In none of the studies published so far has the full potential of the RPH with regard to providing mechanistic insight into a chemical reaction been exploited. An exception is the recent work by Konkoli, Kraka, and Cremer,[63] which concentrates on mechanistic rather than dynamic aspects of the RPH approach. This work will be discussed here.

3.2 The Unified Reaction Valley Analysis: $CH_3 + H_2 \rightarrow CH_4 + H$

A mechanistically oriented investigation based on the RPH comprises two major steps: analysis of the RP and all those properties which are a function of the reaction coordinate s (investigation of the one-dimensional reaction space); analysis of the $(3K - L - 1)$-dimensional vibrational space and all those properties that depend on the $(3K - L - 1)$ normal coordinates (investigation of the $(3K - L - 1)$-dimensional reaction valley). In a particular case, the analysis can consider the following RP and reaction valley properties.

(a) *Investigation of the one-dimensional reaction space*:

(1) The energy profiles $V_0(s)$ and $V_{vap}(s)$ describe the energetics of the reaction (energy barrier, reaction energy).
(2) The geometry changes of the reaction complex as a function of s provide the geometries of reactants, TS, and products as well as all intermediate points along the RP.
(3) The analysis of the RP vector $\boldsymbol{t}(s)$ in terms of internal coordinates reveals which geometrical parameter of the reaction complex dominates the direction of the RP, i.e., the path tangent.
(4) The analysis of the gradient expressed in internal coordinates leads to the internal forces exerted on the nuclei of the reaction complex as a function of s.
(5) The investigation of the electron density distribution $\rho(\boldsymbol{r}, s)$ along the path using difference density distributions $\Delta\rho(\boldsymbol{r}, s)$, Laplace concentrations $-\nabla^2\rho(\boldsymbol{r}, s)$, and other density properties helps to explain changes in the forces and the overall energy along the RP.
(6) The calculation and analysis of various properties of the reaction complex such as dipole moment, polarizability, magnetic susceptibility, etc., as a function of s complements the description.

(b) *Investigation of the $(3K - L - 1)$-dimensional reaction valley*:

(1) Investigation of normal mode frequencies as a function of s leads to the identification of avoided mode–mode crossings and RP bifurcation points.
(2) Modes with a strong dependence on s can be decomposed in terms of adiabatic internal modes to unravel their dependence on certain geometrical features of the reaction complex.
(3) The analysis of adiabatic force constants and adiabatic frequencies associated with the internal coordinates that describe the reaction complex provides direct insight into how the reaction complex changes along s.
(4) Analysis of the RP curvature $\boldsymbol{k}(s)$ helps to identify those path regions with strong curvature and a coupling between translational and transverse vibrational modes. For this purpose, the curvature is investigated in terms of normal mode–curvature coupling coefficients $B_{\mu,s}$ and adiabatic internal mode–curvature coupling amplitudes $A_{k,s}$.
(5) Particular mode–mode coupling coefficients $B_{\mu,\nu}$ are analyzed as a function of s.
(6) A mode–mode coupling pattern is determined to describe possible mechanism of energy dissipation between modes.

A combination of 3.2.1(1–6) and 3.2.2(1–6) leads to a unified description of RP and reaction valley and provides detailed insight into the reaction mechanism. This will be shown in the following for the reaction

$$CH_3 + H_2 \longrightarrow CH_4 + H \qquad (51)$$

since this reaction is a benchmark example for many applications and improvements of the RPH (see Table 3). The internal coordinates of the reaction complex are defined in

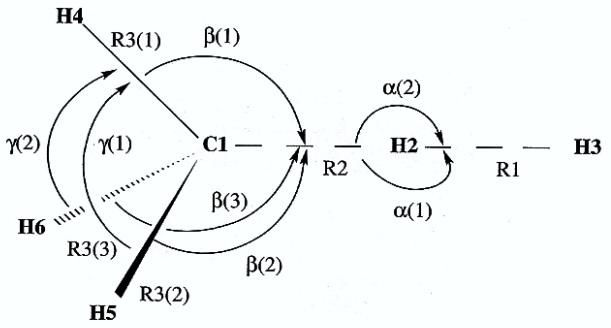

Figure 8 Internal coordinates used to describe the reaction complex $CH_3 \cdots H_2$. Reproduced with permission from Z. Konkoli, E. Kraka, and D. Cremer, *J. Phys. Chem.*, 1997, **101**, 1742-1757. Copyright (1997) American Chemical Society

Figure 8, where a complete set of $(3K - 6)$ coordinates has to be given to apply the RPH. The investigation was carried out with standard UMP2 methodology and a VDZ + P basis set of the 6-31G(p,d) type.[63]

3.2.1 *Investigation of the One-dimensional Reaction Space*

Reaction (51) is known to be exothermic by 3.1 kcal mol^{-1} with an energy barrier of 10 kcal mol^{-1}.[89] UMP2/6-31G(d,p) exaggerates both the exothermicity and the barrier of reaction (51) somewhat as is indicated by calculated energies of -8.1 and 14.2 kcal mol^{-1}. Inclusion of zero-point energy corrections leads to values of -4.6 and 16.2 kcal mol^{-1} and shifts the maximum of the vibrationally adiabatic potential slightly into the entrance channel (Figure 9). The internal coordinates of the reaction complex, which experience the largest changes during the reaction, are the CH distance R2 (before and slightly after the TS), the HH distance R1 (after the TS), and the pyramidalization angle $\beta(s)$ (before and after the TS, see Figure 10). Strong curvature of the functions R1(s) ($-0.2 \leq s \leq 0.3$ $amu^{1/2}$ Bohr) and R2(s) ($0.5 \leq s \leq 0.7$ $amu^{1/2}$ Bohr) indicates that the corresponding bond is beginning to break (R1) or is finishing its formation (R2).

Analysis of the RP vector (Figure 11) reveals that in the entrance channel coordinate R2 is dominating the direction of the RP while R1 is dominating $\boldsymbol{t}(s)$ in the exit channel. This is not surprising, since R2 is the appropriate approach

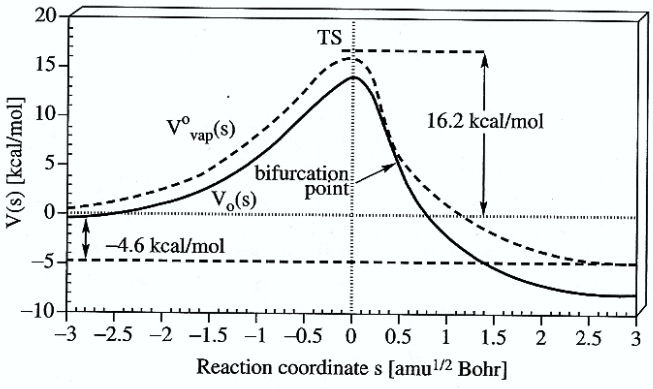

Figure 9 Potential $V_0(s)$ (solid line) and $V^{\circ}_{vap}(s)$ (dashed line) for the reaction $CH_3 + H_2 \rightarrow CH_4 + H$ as calculated at the UMP2/6-31G(d,p) level of theory

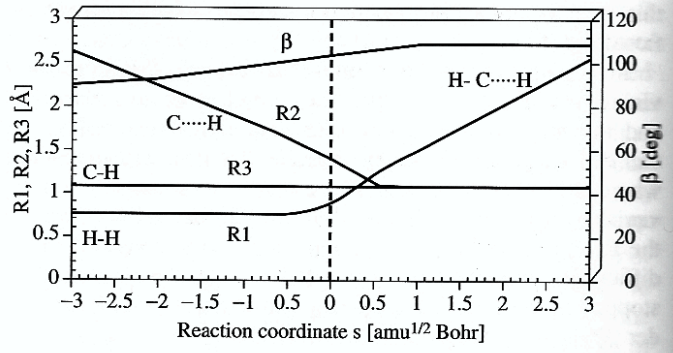

Figure 10 Geometrical parameters of the reaction complex $CH_3 \cdots H_2$ as a function of s

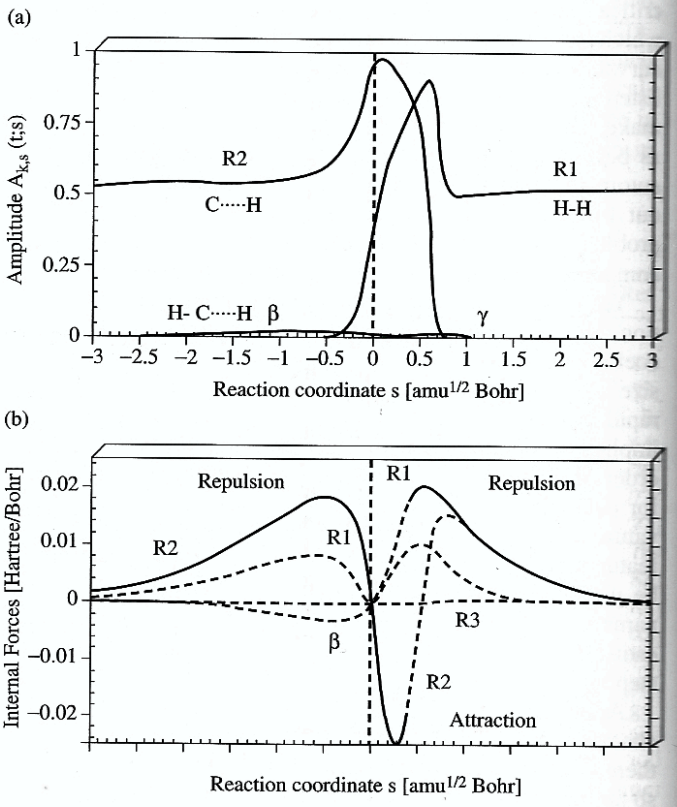

Figure 11 Analysis of reaction path vector $\boldsymbol{t}(s)$ and gradient for the reaction $CH_3 + H_2 \rightarrow CH_4 + H$. (a) Characterization of $\boldsymbol{t}(s)$ in terms of amplitudes $A_{k,s}(t;s)$ (see equation 38). (b) Decomposition of the gradient in terms of attractive and repulsive internal forces. Forces corresponding to the internal coordinate that dominates $\boldsymbol{t}(s)$ in a given range of the RP are indicated by thick solid lines

parameter for $CH_3 + H_2$ while R1 takes the same role for $CH_4 + H$. In the vicinity of the TS, the contributions from R2 and R1 to the RP vector increase to a maximum where the maximum of the amplitude for R2 at the TS is followed by the corresponding maximum for R1 after the TS. The two maxima can be associated with the actual chemical processes, namely the forming of a new CH bond and the breaking of the HH bond.

The amplitudes of the internal coordinate components of the RP vector help to analyze the dependence of the forces on the reaction coordinate s. The forces that drive the reaction

along the RP can be identified as those that are associated with the dominating component of the RP vector as is indicated in Figure 11(b) by thick solid lines. The force between H2 and H3 (parameter R1) before and after the TS is always repulsive, with maximal values at $s = \pm 0.5$. The force between atoms C1 and H2 (parameter R2) increases from its zero value at the equilibrium geometries of the reactants to a maximum of repulsion at $s = -0.5$ before it vanishes at the TS and becomes strongly attractive with a minimum at $s = 0.3$ amu$^{1/2}$ Bohr. In the region between 0.4 and 0.8, R2 and R1 change their role in the RP vector, which is accompanied by an increase of both the R2 and R1 forces to a repulsive maximum. Then in the exit channel all forces decay to the zero values of CH_4 in its equilibrium geometry.

The changes in the forces as a function of s (Figure 11b) can be explained with the help of the electron difference density distributions $\Delta\rho(\boldsymbol{r}, s)$ at selected values of s shown in Figure 12. When the reacting molecules approach each other (Figure 12a, $s = -3$ amu$^{1/2}$ Bohr) the dominant interaction is exchange (overlap) repulsion that leads to a depletion of negative charge in the region between the molecules as indicated by a negative $\Delta\rho(\boldsymbol{r})$ distribution (dashed lines in Figure 12a). Exchange repulsion increases with decreasing R2 value and leads to a maximum in the R2 force. At the same time, both CH_3 and H_2 become polarized so that electron density is shifted from the approach side to the back side of the molecules (Figure 12b, $s = -0.5$ amu$^{1/2}$ Bohr). Induction forces caused by the build up of negative charge at C1 and the induced $H2^{\delta+}$-$H3^{\delta-}$ dipole moment begin to compensate part of the exchange repulsion.

Figure 12(c) gives the situation of the TS, at which attractive induction forces (enlarged by dispersion forces) and repulsive exchange forces exactly compensate each other. At this point, *polarization* of the HH bond has proceeded to a point where a significant amount of electron density flows out of the bond region, i.e., the breaking of the HH bond has started (compare with the upward curving of R1(s) in Figure 10). At the same time, the negative charge at C is polarized in the direction of H_2, which represents the positive end of the HH bond dipole. The two molecules start to attract each other, since the HH bond begins to break and simultaneously a CH bond starts to form (Figure 12d). The R2 force adopts a minimum value half way in this process. In the second half of the bond breaking and bond forming process, the R1 coordinate starts to dominate the RP vector since H2 begins to separate from the forming CH_4 molecule. Exchange repulsion between H_2 and CH_4 becomes important and causes a repulsion maximum in the R1 force.

The analysis of other properties of the reaction complex along s support this description of the reaction mechanism based on the behavior of the RP vector, forces, and electron density distribution. They all suggest that the reaction proceeds through different stages that can clearly be distinguished. This is confirmed by an investigation of the reaction valley.

3.2.2 *Investigation of the Reaction Valley*

Most important for the description of the reaction valley are the harmonic frequencies of the modes orthogonal to the RP. They have to be ordered for all points s considered and then they can be presented as functions $\omega_\mu(s)$ as done in Figure 13 for reaction (51). The labeling of the frequencies

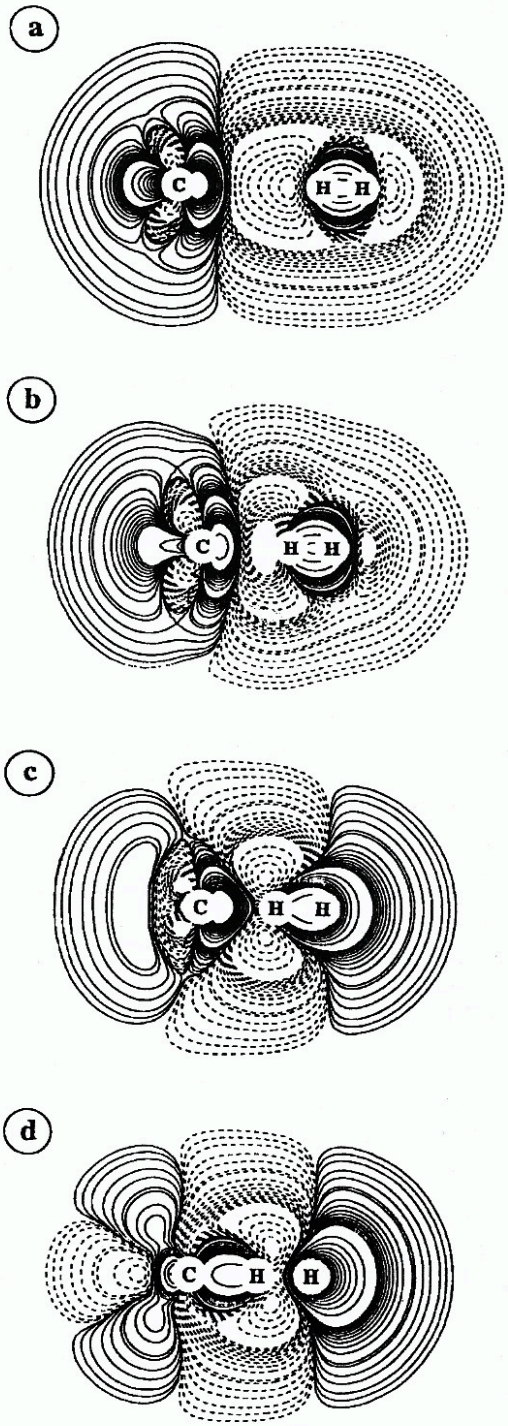

Figure 12 Electron difference density distribution $\Delta\rho(\boldsymbol{r}, s)$ obtained at (a) $s = -3.0$, (b) $s = -0.5$, (c) $s = 0$, and (d) $s = 0.3$ amu$^{1/2}$ Bohr for the reaction $CH_3 + H_2 \rightarrow CH_4 + H$. Solid contour lines indicate an increase, dashed contour lines a decrease of electron density relative to the electron density of the procomplex, i.e., noninteracting CH_3, H_2, CH_4, and H. Reproduced with permission from Z. Konkoli, E. Kraka, and D. Cremer, *J. Phys. Chem.*, 1997, **101**, 1742–1757. Copyright (1997) American Chemical Society

is done considering the C_{3v} symmetry of the reaction complex and the order they have in the entrance channel of the reaction.

The largest changes in $\omega_\mu(s)$ occur for modes 8 and 11, which are both of a_1 symmetry. The adiabatic analysis of these

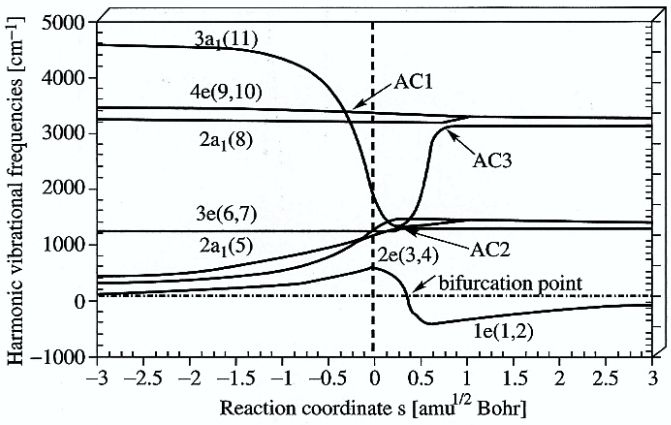

Figure 13 Normal mode frequencies $\omega_\mu(s)$ in cm^{-1} for the reaction $CH_3 + H_2 \rightarrow CH_4 + H$. Symmetry symbols and numbering of normal modes are given according to the order of normal modes calculated for the reactants $CH_3 + H_2$. The value $\omega_{1e}(s) = 0$ indicates the location of the bifurcation point ($s = 0.4$ amu$^{1/2}$ Bohr). Imaginary 1e frequencies calculated for $s > 0.4$ amu$^{1/2}$ Bohr are given as negative numbers. Avoided crossings AC1, AC2, and AC3 are indicated

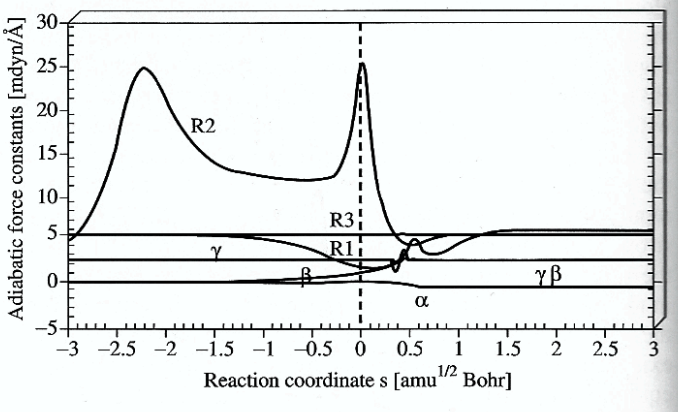

Figure 14 Generalized adiabatic force constants associated with the internal coordinates used to describe the $CH_3 \cdots H_2$ reaction complex (Figure 8)

modes reveals that mode 11 corresponds to HH stretching in the entrance channel and to CH stretching of a spectator bond in the exit channel. These contributions are reverted in the case of mode 8, which first corresponds to CH stretching of the spectator bonds, changes then to HH stretching of the breaking HH bond and, finally, represents CH stretching of the newly formed CH bond. There is an avoided crossing (AC1) between modes 8 and 11 at $s = -0.3$ amu$^{1/2}$ Bohr (Figure 13). Other avoided crossings between modes of a_1 symmetry can be found at $s = 0.35$ (AC2, #5 and 8) and 0.7 amu$^{1/2}$ Bohr (AC3, #8 and 11).

A branching point of the reaction is indicated by $\omega_\mu(s)$ of the degenerate 1e-symmetrical modes (#1 and 2). The harmonic frequencies of these modes become imaginary for $s > 0.4$ amu$^{1/2}$ Bohr (indicated in Figure 13 by negative $\omega_\mu(s)$ values). The reaction valley splits at the branching point into three separated reaction valleys, which correspond to a reduction of the symmetry of the reaction complex from C_{3v} to C_s, i.e., the leaving H atom moves into one of the three positions between two CH bonds of the methane molecule. The energies in the new reaction valleys are just a small fraction of a kcal mol^{-1} below the energy values of the ridge path, for which C_{3v} symmetry of the reaction complex is conserved. This indicates that in this region the RPH concept has to be extended by considering another large amplitude motion, which corresponds to a transfer of the leaving H atom from one valley to the other. However, since the region beyond the bifurcation point is energetically not interesting, most authors have refrained from applying a reaction surface model to this path region.

Adiabatic force constants calculated at equilibrium geometries reflect electronic effects associated with a particular molecular fragment and the internal coordinate describing this fragment. This is no longer true in the case of the generalized adiabatic force constants shown in Figure 14. By construction, they cover two different effects: (a) the curvature of the reaction valley orthogonal to the path direction; (b) the projection effect from $(3K - L)$- to $(3K - L - 1)$-dimensional space.

Konkoli, Kraka, and Cremer[63] have shown that the adiabatic internal modes (as any other local mode) do not necessarily lie in the $(3K - L - 1)$-dimensional (hyper)plane spanned by the normal mode vectors and for which the RP vector $\boldsymbol{t}(s)$ is the normal vector. If the direction of an adiabatic mode vector is more or less orthogonal to the direction of $\boldsymbol{t}(s)$, then its projection onto the $(3K - L - 1)$-dimensional subspace will be dominated by the electronic effect (a). However, if the adiabatic mode vector points in a similar direction to $\boldsymbol{t}(s)$, then its value in $(3K - L - 1)$-dimensional space will be relatively large and mainly due to the projection. This means that a large value of an adiabatic force constant $k_a(s)$ reveals those positions along the RP where the associated internal coordinate becomes (almost) parallel with the RP direction. This complements information obtained from analysis of the vector $\boldsymbol{t}(s)$ (Figure 11a). An exceedingly large adiabatic force constant is found in the case of reaction (51) for the adiabatic mode associated with R2 at the position of the TS and in the entrance channel at $s = -2.2$ amu$^{1/2}$ Bohr (Figure 14). Clearly, the maximum of k_a[R2] at the TS corresponds to the maximum of the R2 amplitude of the RP vector and indicates the beginning of the CH bond formation. The second maximum in the entrance channel has been described as identifying that point at which a first 'preparation' of the reacting molecules for the reaction occurs.[63] Under the impact of the approaching H_2 molecule the CH_3 molecule starts to pyramidalize, which is accompanied by the conversion of a pure π-radical to a σ-radical and a lowering of local D_{3h} to C_{3v} symmetry. The width of the R2-peak at $s = -2.2$ amu$^{1/2}$ Bohr indicates that pyramidalization contrary to bond cleavage is a slow process. This can easily be understood, considering the fact that at a distance of 2–2.5 Å (Figure 10) between the reacting molecules interactions are moderate and only slowly increase with decreasing value of R2.

The adiabatic force constant associated with coordinate R3 does not change during the reaction, indicating that the CH bonds of the CH_3 radical are spectator bonds. The changes in the R1 and bending angle force constants are related to the changes in the RP vector and the bifurcation of the RP.

The RP curvature $k(s)$ (Figure 15) exhibits two distinct peaks in the TS region at $s = -0.1$ and 0.7 amu$^{1/2}$ Bohr (peaks K2 and K3), which are primarily associated with mode 8 and to a lesser extent with modes 5 and 11 as the curvature

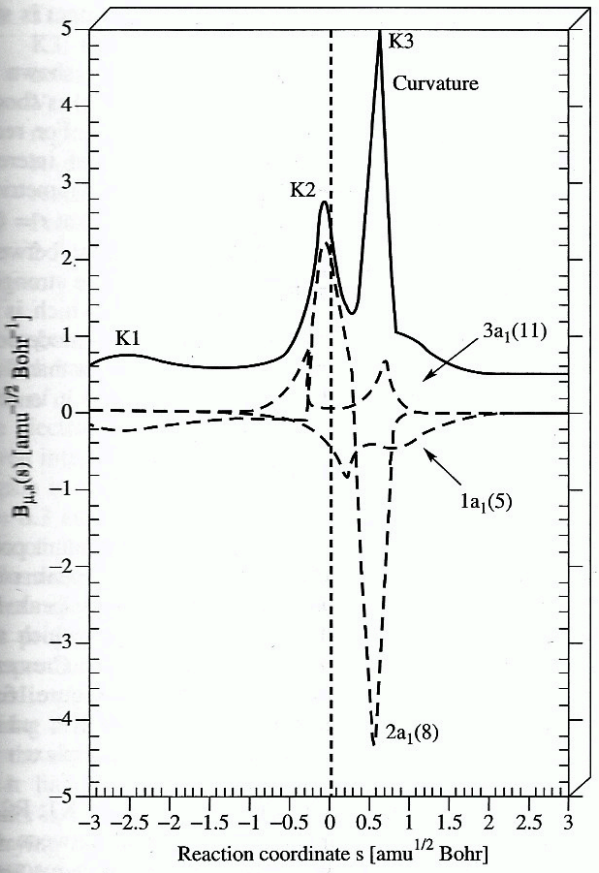

Figure 15 Characterization of the reaction path curvature $k(s)$ (thick solid line) in terms of normal mode–curvature coupling coefficients $B_{\mu,s}(s)$ (dashed lines) for the reaction $CH_3 + H_2 \rightarrow CH_4 + H$. The curve $k(s)$ has been shifted by 0.5 units to more positive values to facilitate the distinction between $k(s)$, and $B_{\mu,s}(s)$. Reproduced with permission from Z. Konkoli, E. Kraka, and D. Cremer, *J. Phys. Chem.*, 1997, **101**, 1742–1757. Copyright (1997) American Chemical Society

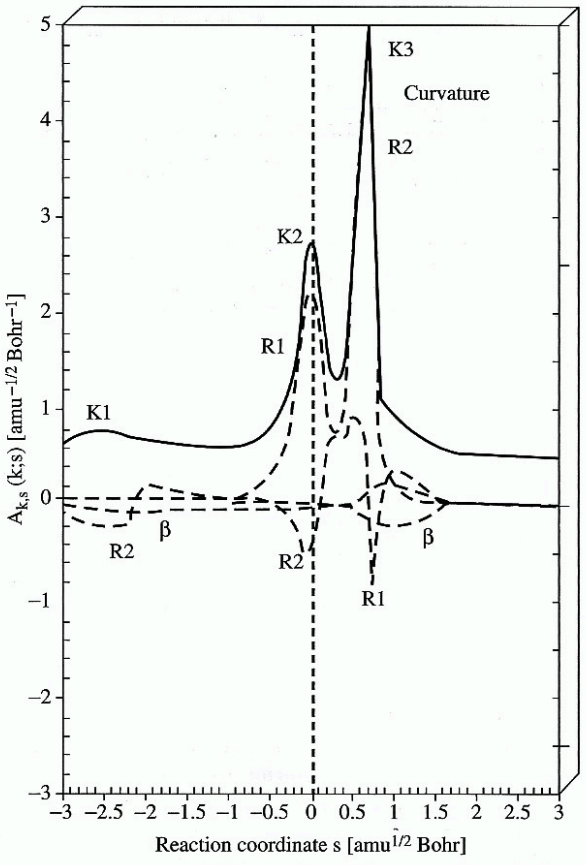

Figure 16 Characterization of the reaction path curvature $k(s)$ (thick solid line) in terms of adiabatic mode–curvature coupling amplitudes $A_{k,s}(\boldsymbol{k};s)$ (dashed lines) for the reaction $CH_3 + H_2 \rightarrow CH_4 + H$. The curve $k(s)$ has been shifted by 0.5 units to more positive values to facilitate the distinction between $k(s)$ and $A_{k,s}(\boldsymbol{k};s)$. Reproduced with permission from Z. Konkoli, E. Kraka, and D. Cremer, *J. Phys. Chem.*, 1997, **101**, 1742–1757. Copyright (1997) American Chemical Society

coupling coefficients reveal. There is also a small curvature maximum at $s = -2.5$ (peak K1, Figure 15) close to the position of the maximum of the generalized adiabatic force constant associated with R2. Decomposition of the curvature in terms of adiabatic mode–curvature coupling amplitudes (Figure 16) shows that peak K1 is indeed dominated by the negative adiabatic R2 component, which means that curvature vector and adiabatic mode vector are collinear but point in opposite directions, indicating that the reacting system resists a shortening of the R2 distance since this implies pyramidalization of CH_3. Once pyramidalization of CH_3 is initiated and attractive induction forces start to develop (see Figure 11b and discussion of forces), the R2 adiabatic mode vector rotates in the direction of the curvature vector $\boldsymbol{k}(s)$ (at $s > -2.2$ amu$^{1/2}$ Bohr). Clearly, the first curvature peak can be associated with the beginning pyramidalization of CH_3 while the region between the first and second curvature peaks is that region in which the reactants are prepared for the actual chemical reaction, namely the bond breaking and forming process of reaction (51).

The second curvature peak is dominated by the R1 component, thus indicating that the HH bond is beginning to break. The maximum in the R2 component of the RP vector, as well as the maximum in the adiabatic force constant k_a[R2], suggest that HH bond cleavage is parallel to CH bond formation (coordinate R2). These two processes seem to be essentially finished at $s = 0.6$ amu$^{1/2}$ Bohr as indicated by the third curvature peak, which is dominated by the R2 component. Peak K3 identifies the point where the CH bond forming process will be basically finished if the forward reaction $CH_3 + H_2$ is considered; for the reverse reaction $CH_4 + H$, it is the point where bond C1H2 starts to cleave.

If one considers the changes in $k(s)$ (Figure 16) parallel to those in $t(s)$ (Figure 11a) and $k_a(s)$ (Figure 14), a clear picture of the HH bond breaking and CH bond forming process will emerge. These processes occur in the region of curvature peaks K2 and K3 ($-0.1 < s < 0.6$) as indicated by maxima or minima of the amplitudes associated with the internal parameters R1 and R2 describing these bonds, by the maxima of the R2 and R1 amplitudes of the RP vector, and the TS maximum of the adiabatic force constant k_a[R2] (and a smaller one of k_a[R1]).

Mode–mode couplings that decide the exchange of energy between different modes are particularly large at the positions of avoided crossings as is shown in Figure 17 in the case of the coupling coefficient between the a_1-symmetrical modes

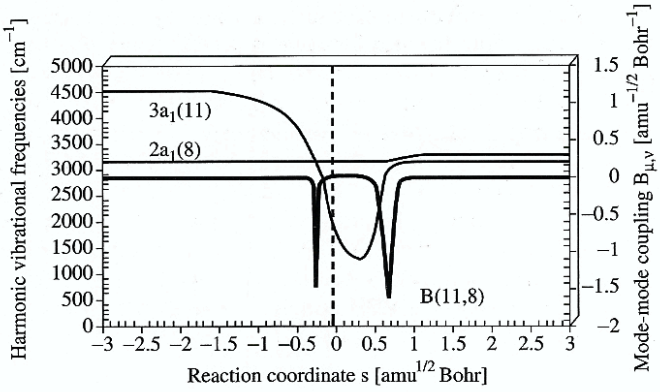

Figure 17 Normal mode frequencies $\omega_\mu(s)$ of the $3a_1$ and $2a_1$ symmetric mode (#11 and 8) and the corresponding Coriolis coupling coefficient $B_{11,8}(s)$ for the reaction $CH_3 + H_2 \rightarrow CH_4 + H$. Reproduced with permission from Z. Konkoli, E. Kraka, and D. Cremer, *J. Phys. Chem.*, 1997, **101**, 1742–1757. Copyright (1997) American Chemical Society

11 and 8. There are distinct coupling peaks at the positions of the two avoided crossings. In line with the discussion of the $\omega_\mu(s)$ curves (Figure 13), interactions between the two a_1-modes are relatively weak at $s = -0.3$ amu$^{1/2}$ Bohr while they are stronger at $s = 0.6$ amu$^{1/2}$ Bohr (Figure 17).

Significant mode–mode coupling leads to energy dissipation from one vibrational mode to the other. This will be of importance if one tries to enhance the reaction rate by channeling energy into vibrational mode 11 (e.g., by tuning a laser to the frequency ω_{11} of the reactants) that couples with the reaction mode in the entrance channel, as revealed by the RP curvature $k(s)$ (Figure 15). Part of this energy will be dissipated into vibrational mode 8 because of the 8,11-coupling at $s = -0.3$ amu$^{1/2}$ Bohr (Figure 17). However, since the coupling is strongly localized, energy dissipation will be small so that the rate enhancement is still effective.

A condensed mode–mode coupling pattern is shown in Figure 18, in which only the largest value of $B_{\mu,\nu}(s)$ is shown for each combination of normal modes l_μ and l_ν. For reaction (51), there are just two couplings that are of interest, namely the coupling between the $1a_1$- and $2a_1$-symmetrical mode (modes 5 and 8, $B_{5,8} = 12.2$ amu$^{-1/2}$ Bohr^{-1}) at $s = 0.3$ amu$^{1/2}$ Bohr and the one at $s = 0.7$ amu$^{1/2}$ Bohr between modes 8 ($2a_1$) and 11 ($3a_1$) (Figure 17). Clearly, the strongest energy dissipation will involve modes 5 and 8, which is of relevance for the reverse reaction. All other mode–mode couplings (shown in the inserts of Figure 18) are smaller than 0.05 amu$^{-1/2}$ Bohr^{-1} and, therefore, play a minor role in energy dissipation.

3.2.3 *Discussion of the Reaction Mechanism*

Although the TS is energetically the most important point of the reaction, mechanistically it is better to speak of a transition state region that reaches from curvature peak K2 to peak K3 and defines that part of the RP in which the major chemical changes occur. Konkoli, Kraka, and Cremer[63] have suggested using the curvature diagram of Figure 16 to distinguish between different regions along the RP, which correspond to different changes of the reaction complex:

(1) Reactant region (to the left of curvature peak K1; R2 > 2.5 Å): There are only weak interactions between the reactants without any chemical relevance; the reactants possess electronic structures that basically correspond to those of their equilibrium geometries.

(2) Van der Waals region on reactant side ('preparation region' between curvature peaks K1 and K2): The reactants prepare for the reaction under the impact of increasing interactions; pyramidalization of CH_3 and polarization of H_2 occurs.

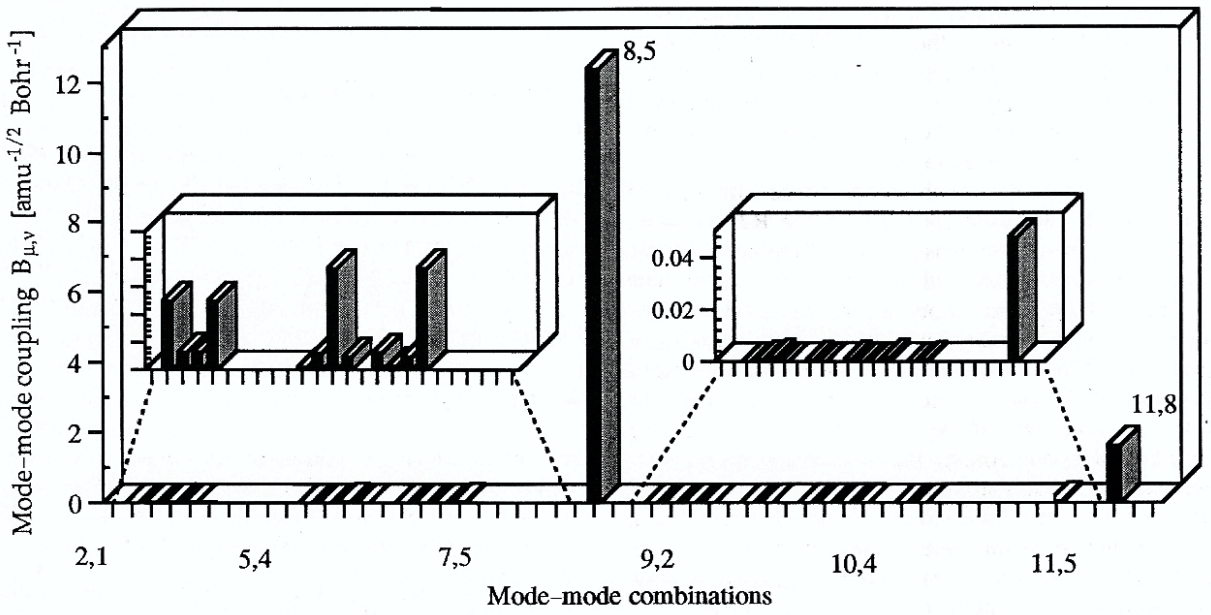

Figure 18 Mode–mode coupling pattern for the reaction $CH_3 + H_2 \rightarrow CH_4 + H$. The largest value of the coefficient $B_{\mu,\nu}(s)$ is given for each of the 55 possible mode combinations. Reproduced with permission from Z. Konkoli, E. Kraka, and D. Cremer, *J. Phys. Chem.*, 1997, **101**, 1742–1757. Copyright (1997) American Chemical Society

(3) Transition state region (between curvature peaks K2 and K3; see Figure 16): Bonds are broken or formed. The actual chemical reaction takes place.
(4) Van der Waals region on the product side ('finalization region' for the forward or 'preparation' region for the reverse reaction): The products prepare for the reverse reaction under the impact of increasing interactions.
(5) Product region (to the right of curvature peak K3; R1 > 2 Å): Very weak interactions between products without any chemical relevance.

In general, it will be easy to identify the TS region because it is characterized by large curvature peaks where the magnitude of a curvature peak may be related to the magnitude of the electronic structure changes accompanying changes in a given internal coordinate. In the case of reaction (51), the TS region is not centered at the location of the TS, but shifted to $s = 0.3$ amu$^{1/2}$ Bohr (Figure 16), which means that the position of the TS is shifted from the center of the TS region to the entrance channel of the reaction. Obviously, this displacement reflects the fact that for an exothermic reaction the TS has properties closer to those of the reactants than those of the products ('early TS') in line with the Hammond postulate. This implies that the strong electronic changes that take place during a reaction are just initiated at the TS as is confirmed by the analysis of $\boldsymbol{k}(s)$ and $\boldsymbol{t}(s)$.

It has been suggested that the height of the curvature peaks is related to the resistance of the reaction complex to carrying out the electronic structure changes associated with bond breaking or bond forming. HH bond breakage in the forward reaction is much easier than CH bond breakage in the reverse reaction, which is directly related to the fact that mutual polarization of H_2 and CH_3 (peak K1 in the van der Waals region) is much easier than mutual polarization of CH_4 and H (no extra curvature peak in the exit channel). The height of the R2-dominated curvature peak K3 is almost twice as large as that of the R1-dominated curvature peak K2, which can be related to calculated energy barriers (Figure 9) of 16 kcal mol^{-1} in the forward reaction and 21 kcal mol^{-1} in the reverse reaction. Hence, the ratio of the heights of the curvature peaks K2 and K3 together with the position of the TS in the TS region directly reveals the exothermic nature of the reaction and the nature of the TS as an early TS shifted by 0.3 amu$^{1/2}$ Bohr into the entrance channel.

The van der Waals region on the product side ('finalization region') is reduced to just a shoulder of the R2 curvature peak in the exit channel as a consequence of the considerable stiffness of the CH_4 molecule with regard to interactions with the incoming H atom. The shoulder of the R2-dominated curvature peak K3 is associated with the R1 and β adiabatic vibrational modes (Figure 16) and can be discussed in terms of a reduction of the HH distance and a local symmetry lowering from T_d to C_{3v} symmetry of the CH_4 molecule (considering the reverse reaction). Of course, this interpretation can only be qualitative since the path region in question is beyond the bifurcation point and, therefore, represents a ridge path between three new reaction valleys. In such a situation the RPH has to be extended to a reaction surface, which is not interesting because of the minor energy changes occurring in this part of the PES.

If one considers just the energy profile of Figure 9 and the geometry diagram of Figure 10, reaction (51) will have a rather simple mechanism characterized just by a breaking of the HH and a simultaneous forming of the CH bond. However, a detailed analysis based on the RPH and summarized in Figures 9 to 18 provides many insights that lead to a new understanding of the reaction mechanism. Most important is the description of electronic structure changes occurring in the van der Waals region, since these prepare the reactants for the actual bond breaking/forming processes. With the help of the RPH approach one can exactly specify when *van der Waals interactions* become relevant for the reaction mechanism. Hence, the RPH concept provides the basis for a complete mechanistic description of reaction (51).

4 CONCLUSIONS

The reaction path Hamiltonian (RPH) is the basis of a powerful concept for investigating both the mechanism and the dynamics of a chemical reaction. Its application requires the handling of a number of computational techniques and a relatively large amount of computer time. Progress in the development of appropriate methods to find the stationary points of a PES, to follow the RP, to detect branching points of the RP and to calculate all quantities of the RPH has made it possible to apply the RPH routinely nowadays even for larger reaction systems. A number of techniques is available to keep computational cost at a reasonable level even when more accurate correlation-corrected methods are applied. The usefulness of the RPH for determining the dynamics of a chemical reaction has been demonstrated in many cases. However, its potential for providing detailed mechanistic insights into reactions is still not fully exploited although recent work in this direction is very promising.

Clearly, the RPH is based on a number of assumptions and, therefore, it cannot be applied to all chemical reactions. Improvements and modifications of the original RPH have been suggested that extend the range of applicability considerably. Nevertheless, more development work is needed in this area.

5 RELATED ARTICLES

Coupled-cluster Theory; Density Functional Theory (DFT), Hartree–Fock (HF), and the Self-consistent Field; Geometry Optimization: 1; Geometry Optimization: 2; Mixed Quantum–Classical Methods; Møller–Plesset Perturbation Theory; Rates of Chemical Reactions; Reaction Path Following; Transition State Theory; Unimolecular Reaction Dynamics.

6 REFERENCES

1. A. H. Zewail, in 'Femtosecond Chemistry', eds. J. Manz and L. Wöste, VCH, Weinheim, 1995, pp. 15–128.
2. D. G. Truhlar (ed.), 'Potential Energy Surfaces and Dynamics Calculations', Plenum Press, New York, 1981.
3. J. N. Murrell, S. Carter, S. C. Farantos, P. Huxley, and A. J. C. Varandas, 'Molecular Potential Energy Functions', Wiley, New York, 1984.
4. W. H. Miller, N. C. Handy, and J. E. Adams, *J. Chem. Phys.*, 1980, **72**, 99–112.
5. K. Fukui, *Acc. Chem. Res.*, 1981, **14**, 363–368.

6. V. Barone and C. Minichino, *J. Mol. Struct. (Theochem.)*, 1995, **330**, 365–376.
7. A. Nauts and X. Chapuisat, *Chem. Phys.*, 1983, **76**, 349–366.
8. T. Carrington, Jr. and W. H. Miller, *J. Chem. Phys.*, 1984, **81**, 3942–3949.
9. D. G. Truhlar, R. Steckler, and M. S. Gordon, *Chem. Rev.*, 1987, **84**, 217–236.
10. S. Lee and J. T. Hynes, *J. Chem. Phys.*, 1988, **88**, 6853–6862; 1988, **88**, 6863–6869.
11. C. J. Espinosa-Garcia, W.-P. Wu, I. Rossi, and D. G. Truhlar, *J. Phys. Chem.*, 1995, **99**, 687–694.
12. A. A. Viggiano, J. S. Paschkewitz, R. A. Morris, J. F. Paulson, A. Gonzalez-Lafont, and D. G. Truhlar, *J. Am. Chem. Soc.*, 1991, **113**, 9404–9405.
13. G. H. Peslherbe and W. L. Hase, *J. Chem. Phys.*, 1996, **104**, 7882–7894.
14. J. N. Murrell and K. L. Laidler, *Trans. Faraday Soc.*, 1968, **64**, 371–377.
15. P. G. Mezey, *J. Mol. Struct. (Theochem.)*, 1987, **49**, 57–66.
16. M. V. Basilevsky, *Chem. Phys.*, 1982, **67**, 337–346.
17. H. B. Schlegel, in '*Ab initio* Methods in Quantum Chemistry, Part I', ed. K. P. Lawley, Wiley, New York, 1987, pp. 249–286.
18. T. Schlick, in 'Reviews in Computational Chemistry', Vol. 3, eds. K. B. Lipkowitz and D. B. Boyd, VCH, Weinheim, 1992, pp. 1–71.
19. M. L. McKee and M. Page, in 'Computational Chemistry', Vol. 4, eds. K. B. Lipkowitz and D. B. Boyd, VCH, Weinheim, 1992, pp. 35–65.
20. J. Gauss and D. Cremer, *Adv. Quantum Chem.*, 1992, **27**, 205–299.
21. Y. Yamaguchi, Y. Osamura, J. D. Goddard, and H. F. Schaefer, 'A New Dimension to Quantum Chemistry: Analytical Derivative Methods in *Ab initio* Molecular Electronic Structure Theory', Oxford University Press, Oxford, 1994.
22. W. H. Press, B. P. Flannery, S. A. Teukolsky, and W. T. Vetterling, 'Numerical Recipes, The Art of Scientific Computing', Cambridge University Press, New York, 1986.
23. P. E. Gill, W. Murray, and M. H. Wright, 'Practical Optimization', Academic Press, New York, 1981.
24. J. Simons, P. Jorgensen, H. Taylor, and J. Ozment, *J. Phys. Chem.*, 1983, **87**, 2745–2753.
25. N. Banerjee, N. Adams, J. Simons, and R. Shepard, *J. Phys. Chem.*, 1985, **89**, 52–57.
26. J. Baker, *J. Comput. Chem.*, 1986, **7**, 385–395.
27. C. J. Cerjan and W. H. Miller, *J. Chem. Phys.*, 1981, **75**, 2800–2806.
28. D. Heidrich (ed.), 'The Reaction Path in Chemistry: Current Approaches and Perspectives', Kluwer, Academic, London, 1995.
29. E. Kraka and T. H. Dunning, Jr., in 'Advances in Molecular Electronic Structure Theory', Vol. 1, ed. T. H. Dunning, Jr., JAI Press, London, 1990, pp. 129–173.
30. K. Müller, *Angew. Chem., Int. Ed. Engl.*, 1980, **19**, 1.
31. E. A. McCullough, Jr. and D. M. Silver, *J. Chem. Phys.*, 1975, **62**, 4050–4052.
32. M. Sana, G. Reckinger, and G. Leroy, *Theor. Chim. Acta*, 1981, **58**, 145–153.
33. M. A. Eliason and J. O. Hirschfelder, *J. Chem. Phys.*, 1959, **30**, 1426–1436.
34. See, e.g., K. Yamashita, T. Yamabe, and K. Fukui, *Theor. Chim. Acta*, 1982, **60**, 523–533.
35. See, e.g., H. Goldstein, 'Classical Mechanics', 2nd edn., Addison-Wesley, London, 1980.
36. C. Eckart, *Phys. Rev.*, 1937, **47**, 552–559.
37. See, e.g., D. Laugwitz, 'Differential and Riemannian Geometry', Academic Press, New York, 1965.
38. E. B. Wilson, Jr., J. C. Decius, and P. C. Cross, 'Molecular Vibrations, the Theory of Infrared and Raman Vibrational Spectra', Dover, New York, 1980.
39. A. Tachibana and K. Fukui, *Theor. Chim. Acta*, 1980, **57**, 81–94.
40. A. Igawa and H. Fukutome, *Chem. Phys. Lett.*, 1987, **133**, 399–404.
41. R. G. Pearson, 'Symmetry Rules for Chemical Reactions', Wiley, New York, 1976.
42. M. Page and J. W. McIver, Jr., *Chem. Phys.*, 1988, **88**, 922–935.
43. H. B. Schlegel, *J. Chem. Soc., Faraday Trans.*, 1994, **90**, 1569–1574.
44. V. S. Melissas and D. G. Truhlar, *J. Chem. Phys.* 1992, **96**, 5758–5772.
45. K. Ishida, K. Morokuma, and A. Komornicki, *J.Chem. Phys.*, 1977, **66**, 2153–2156.
46. M. W. Schmidt, M. S. Gordon, and M. Dupuis, *J. Am. Chem. Soc.*, 1985, **107**, 2585–2589.
47. C. Gonzales and H. B. Schlegel, *J. Chem. Phys.*, 1989, **90**, 2154; *J. Phys. Chem.*, 1990, **94**, 5523–5527.
48. R. E. Stanton and J. W. McIver, Jr., *J. Am. Chem. Soc.*, 1975, **97**, 3632–3646.
49. H. Metiu, J. Ross, R. Silbey, and T. F. George, *J. Chem. Phys.*, 1974, **61**, 3200–3209.
50. J. Baker and P. M. W. Gill, *J. Comput. Chem.*, **9**, 465–475.
51. T. Takesugu, N. Tajima, and K. Hirao, *J. Chem. Phys.*, 1996, **105**, 1933–1939.
52. G. L. Hofacker, *Z. Naturforsch.*, 1963, **18a**, 607–619.
53. R. A. Marcus, *J. Chem. Phys.*, 1966, **45**, 4493; 1966, **45**, 4500–4504; 1969, **49**, 2610–2616.
54. S. F. Fischer and M. A. Ratner, *J. Chem. Phys.*, 1972, **57**, 2769–2776.
55. P. Russeger and J. Brickmann, *J. Chem. Phys.*, 1975, **62**, 1086–1093.
56. J. T. Hougen, P. R. Bunker, and J. W. C. Johns, *J. Mol. Spectrosc.*, 1973, **45**, 120–141.
57. D. G. Truhlar, A. D. Isaacson, and B. C. Garrett, in 'Theory of Chemical Reaction Dynamics', ed. M. Baer, CRC Press, Boca Raton, FL, pp. 65–173.
58. S. Kato and K. Morokuma, *J. Chem. Phys.*, 1980, **73**, 3900–3914.
59. J. C. Polany and W. H. Wong, *J. Chem. Phys.*, 1969, **51**, 1439.
60. See, e.g., W. H. Miller, *Chem. Rev.*, 1987, **87**, 19.
61. Z. Konkoli, E. Kraka, and D. Cremer, *J. Comput. Chem.*, 1997, **18**, 1282–1294.
62. (a) Z. Konkoli and D. Cremer, *Int. J. Quantum Chem.*, 1998, **67**, 1–9; (b) Z. Konkoli, J. A. Larsson, and D. Cremer, *Int. J. Quantum Chem.*, 1998, **67**, 11–27; (c) Z. Konkoli and D. Cremer, *Int. J. Quantum Chem.*, 1998, **67**, 29–40.
63. Z. Konkoli, E. Kraka, and D. Cremer, *J. Phys. Chem. A*, 1997, **101**, 1742–1757.
64. S. M. Colwell and N. C. Handy, *J. Chem. Phys.*, 1985, **82**, 1281–1290.
65. C. Minichino and V. Barone, *J. Chem. Phys.*, 1994, **100**, 3717–3741.
66. W. H. Miller, B. A. Ruf, and Y. T. Chang, *J. Chem. Phys.*, 1988, **89**, 6298–6304.
67. W. H. Miller, in 'Theory of Chemical Reaction Dynamics', ed. D. C. Clary, Reidel, Dordrecht, 1986, pp. 27–45.
68. See, e.g., J. Manz and Y. Römelt, *Chem. Phys. Lett.*, 1981, **81**, 179–184.
69. S. D. Schwartz and W. H. Miller, *J. Chem. Phys.*, 1982, **77**, 2378–2382.
70. T. Carrington, Jr. and W. H. Miller, *J. Chem. Phys.*, 1986, **84**, 4364–4370.
71. N. Shida, P. F. Barbara, and J. Almlöf, *J. Chem. Phys.*, 1991, **94**, 3633–3643.
72. T. Tacketsugu and M. S. Gordon, *J. Chem. Phys.*, 1996, **104**, 2835–2840.
73. G. D. Billing, *Chem. Phys.*, 1984, **89**, 199–218; 1989, **135**, 423–436; 1990, **146**, 63–77; 1992, **159**, 109–126.

74. S. K. Gray and W. H. Miller, *J. Chem. Phys.*, 1980, **73**, 2733–2739.
75. B. A. Waite, S. K. Gray, and W. H. Miller, *J. Chem. Phys.*, 1983, **78**, 259–265.
76. T. H. Dunning, Jr., E. Kraka, and R. A. Eades, *Faraday Discuss. Chem. Soc.*, 1987, **84**, 427–440.
77. T. H. Dunning, Jr., L. B. Harding, and E. Kraka, in 'NATO Advanced Research Workshop on Supercomputer Algorithms for Reactivity, Dynamics and Kinetics of Small Molecules', Kluwer, Dordrecht, 1989, 57–71.
78. K. K. Baldrige, M. S. Gordon, R. Steckler, and D. G. Truhlar, *J. Chem. Phys.*, 1989, **93**, 5107–5119.
79. V. M. Ryaboy, *Chem. Phys. Lett.*, 1989, **159**, 371–375.
80. N. Rom, V. M. Ryaboy, and N. Moiseyev, *Chem. Phys. Lett.*, 1993, **204**, 175–182.
81. T. N. Truong, *J. Chem. Phys.*, 1994, **100**, 8014–8025.
82. T. N. Truong and W. J. Duncan, *Chem. Phys.*, 1994, **101**, 7408–7414.
83. R. Liu, S. Ma, and Z. Li, *Chem. Phys. Lett.*, 1994, **219**, 143–150.
84. D.-C. Fang and X.-Y. Fu, *Int. J. Quantum Chem.*, 1994, **49**, 3–10.
85. V. M. Mamaev, I. P. Gloriozov, S. Ya. Ishchenko, V. V. Simonyan, E. M. Myshakin, A. V. Prisyajnyuk, and Y. A. Ustynyuk, *J. Chem. Soc., Faraday Trans.*, 1995, **91**, 3779–3782.
86. J. C. Corchado and J. Espinosa-Garcia, *J. Chem. Phys.*, 1996, **105**, 3152–3159.
87. E. Kraka, unpublished.
88. See, e.g., (a) B. G. Johnson, C. A. Gonzales, P. M. W. Gill, and J. A. Pople, *Chem. Phys. Lett.*, 1994, **221**, 100; (b) J. Baker, J. Andzelm, M. Muir, and P. R. Taylor, *Chem. Phys. Lett.*, 1995, **237**, 53.
89. See, e.g., E. Kraka, J. Gauss, and D. Cremer, *J. Chem. Phys.*, 1993, **99**, 5306–5315.

Reaction Profile

See ***Reaction Path Following; Reaction Path Hamiltonian and its Use for Investigating Reaction Mechanisms; Transition State Theory; Transition States in Organic Chemistry: Ab Initio;*** and ***Transition Structure Optimization Techniques***.

Reactive Scattering of Polyatomic Molecules

David C. Clary

University College London, UK

Abbreviations

DVR = discrete variable representation; LEPS = London–Eyring–Polanyi–Sato; NIP = negative imaginary potential; PODVR = potential optimized DVR; QCT = quasiclassical trajectories; RBA = rotating bond approximation; TST = transition state theory.

1 INTRODUCTION

Theory and calculations on the chemical reactions of polyatomic molecules are very active areas of research.[1–3] There are several reasons for this. The most modern experimental techniques using lasers and molecular beams are being applied to study the microscopic details of such chemical reactions including how different vibrational modes of polyatomic molecules influence reactivity,[4] and measurements of the lifetimes of reaction complexes.[5] State-selected experiments of this type require detailed quantum reactive scattering theory in their interpretation. Furthermore, there is a need for the accurate calculation of kinetic data such as rate constants of polyatomic reactions that are sometimes difficult to study in the laboratory but are important in areas such as atmospheric, combustion, and interstellar chemistry.

Advances in quantum chemistry and scattering theory have enabled essentially exact calculations to be performed on very simple reactions of atoms with diatomic molecules such as[6,7]

$$H + H_2 \longrightarrow H_2 + H$$

and the methods used can be extended to reactions of polyatomic molecules.[8] A rigorous theoretical treatment would normally involve three stages: (i) the accurate *ab initio* calculation of energies for many different geometries of the interacting atoms, (ii) fitting the calculated energy points to a suitable potential energy function, and (iii) performing scattering calculations (ideally using quantum mechanics) with this fitted potential energy surface. Parts (i) and (ii) of this procedure are fully discussed in other articles in this encyclopedia. Furthermore, part (iii) is discussed in detail elsewhere for the quantum theory of atom–diatom reactions (see ***State to State Reactive Scattering***) and other articles also discuss scattering calculations on polyatomic reactions using classical and semiclassical methods (see ***Classical Trajectory Simulations: Final Conditions*** and ***Mixed Quantum–Classical Methods***). Here, therefore, we mainly concentrate on the quantum scattering theory for reactions of polyatomic molecules (with polyatomic meaning a molecule with three or more atoms). Also, we emphasize reactions studied at the quantum state-to-state level as theories for the direct calculation of rate constants are also described in another article (see ***Rates of Chemical Reactions***).

Consider a reaction involving four atoms, such as

$$AB(v, j) + CD(v, j') \longrightarrow ABC(n_1, n_2, n_3) + D$$

where v and v' are vibrational levels and j and j' rotational levels of the diatomics AB and CD, while n_1, n_2, and n_3 are quantum numbers for the symmetric stretch, bending, and